Available online at www.sciencedirect.com

SciVerse ScienceDirect

Geochimica et Cosmochimica Acta 75 (2011) 7257–7276

Geochimica et Cosmochimica Acta

www.elsevier.com/locate/gca

Early diagenesis of redox-sensitive trace metals in the Peru upwelling area – response to ENSO-related oxygen fluctuations in the water column

Florian Scholz *, Christian Hensen, Anna Noffke, Anne Rohde, Volker Liebetrau, Klaus Wallmann

Leibniz Institute of Marine Sciences, IFM-GEOMAR, Marine Biogeochemistry, Wischhofstraße 1-3, D-24148 Kiel, Germany

Received 11 April 2011; accepted in revised form 2 August 2011; available online 9 August 2011

Abstract

Pore water and solid phase data for redox-sensitive metals (Mn, Fe, V, Mo and U) were collected on a transect across the Peru upwelling area (11°S) at water depths between 78 and 2025 m and bottom water oxygen concentrations ranging from ~0 to 93 μM. By comparing authigenic mass accumulation rates and diffusive benthic fluxes, we evaluate the respective mechanisms of trace metal accumulation, retention and remobilization across the oxygen minimum zone (OMZ) and with respect to oxygen fluctuations in the water column related to the El Niño Southern Oscillation (ENSO).

Sediments within the permanent OMZ are characterized by diffusive uptake and authigenic fixation of U, V and Mo as well as diffusive loss of Mn and Fe across the benthic boundary. Some of the dissolved Mn and Fe in the water column re-precipitate at the oxycline and shuttle particle-reactive trace metals to the sediment surface at the lower and upper boundary of the OMZ. At the lower boundary, pore waters are not sufficiently sulfidic as to enable an efficient authigenic V and Mo fixation. As a consequence, sediments below the OMZ are preferentially enriched in U which is delivered via both in situ precipitation and lateral supply of U-rich phosphorites from further upslope. Trace metal cycling on the Peruvian shelf is strongly affected by ENSO-related oxygen fluctuations in bottom water. During periods of shelf oxygenation, surface sediments receive particulate V and Mo with metal (oxyhydr)oxides that derive from both terrigenous sources and precipitation at the retreating oxycline. After the recurrence of anoxic conditions, metal (oxyhydr)oxides are reductively dissolved and the hereby liberated V and Mo are authigenically removed. This alternation between supply of particle-reactive trace metals during oxic periods and fixation during anoxic periods leads to a preferential accumulation of V and Mo compared to U on the Peruvian shelf. The decoupling of V, Mo and U accumulation is further accentuated by the varying susceptibility to re-oxidation of the different authigenic metal phases. While authigenic U and V are readily re-oxidized and recycled during periods of shelf oxygenation, the sequestration of Mo by authigenic pyrite is favored by the transient occurrence of oxidizing conditions.

Our findings reveal that redox-sensitive trace metals respond in specific manner to short-term oxygen fluctuations in the water column. The relative enrichment patterns identified might be useful for the reconstruction of past OMZ extension and large-scale redox oscillations in the geological record.

* Corresponding author. Tel.: +49 431 600 2562; fax: +49 431 6002928.

E-mail address: fscholz@ifm-geomar.de (F. Scholz).

0016-7037/$ - see front matter © 2011 Elsevier Ltd. All rights reserved.
doi:10.1016/j.gca.2011.08.007

1. INTRODUCTION

1.1. Scientific conception

It is generally accepted that the accumulation of redox-sensitive metals in marine sediments is primarily controlled by bottom water oxygen concentrations classifying the respective environment into oxic (>63 μM O_2), hypoxic (<63 μM O_2), anoxic (0 μM O_2) or anoxic-sulfidic (0 μM O_2, >0 μM H_2S) (classification after Middelburg and Levin, 2009). The fixation or liberation of metals is mostly due to the differing solubility of oxidized and reduced species. In other words, interaction between sediment pore waters and minerals is the ultimate reason for most trace metal enrichments or depletions with respect to the detrital background. Much of our knowledge on the behavior of redox-sensitive metals in oceanic pore waters has been deduced at oxic and hypoxic sites in the N Atlantic and N Pacific margins (e.g. Klinkhammer and Palmer, 1991; Shaw et al., 1994; Zheng et al., 2000; Chaillou et al., 2002; Zheng et al., 2002a; McManus et al., 2005; Morford et al., 2005) as well as in anoxic-sulfidic basins with restricted water column circulation such as the Cariaco Trench and the Black Sea (e.g. Anderson et al., 1989a,b; Barnes and Cochran, 1990; Emerson and Huested, 1991). To date, no systematic studies on the pore water chemistry of trace metals have been carried out in the pronounced eastern boundary oxygen minimum zones (OMZs) of the southern Pacific and Atlantic. This is a remarkable gap, considering that these regions strongly differ from the aforementioned systems regarding their water column circulation pattern and/or the extent of detrital input, primary productivity and oxygen depletion. The Peru upwelling system is of additional interest, since it is strongly affected by oceanographic large-scale perturbations related to the El Niño Southern Oscillation (ENSO). Understanding the influence of ENSO-related annual and interannual oscillations in bottom water redox conditions on trace metal cycling is not possible based on solid phase geochemical data alone, but necessitates a thorough examination of pore water profiles.

The trace metals studied here, V, Mo and U, are widely used as paleo-redox indicators (e.g. Brumsack, 2006; Tribovillard et al., 2006; Algeo and Tribovillard, 2009). A detailed understanding of how they respond to transient re-oxidation and redox oscillations is an important prerequisite to identify similar environmental conditions in the geological record. Moreover, climate change and anthropogenically induced eutrophication will lead to an increasing occurrence of seasonal or perennial shelf hypoxia in the coming decades (Diaz, 2001; Diaz and Rosenberg, 2008; Stramma et al., 2008). Trace element cycling in the dynamic Peruvian OMZ may therefore serve as a paradigm for future scenarios in which high-amplitude oxygen fluctuations such as those related to ENSO will occur more frequently.

In this article we discuss sediment and pore water data for V, Mo, U and related redox species (Mn, Fe, H_2S) that were collected on a transect across the Peruvian OMZ at 11°S. The comparison of authigenic mass accumulation rates and diffusive benthic fluxes enables a quantitative evaluation of the respective mechanisms of trace metal accumulation and retention or remobilization. Finally, we discuss implications for the use of U–Mo systematics as a paleo-proxy for oxygen fluctuations in bottom water and combine our results in a conceptual model, illustrating the lateral and temporal variability of V, Mo and U diagenesis across the Peru upwelling area.

1.2. Marine geochemistry of vanadium, molybdenum and uranium

The three trace metals studied here share many chemical characteristics giving rise to their joint enrichment in oxygen-deficient sediment facies. There are, however, subtle differences in their diagenetic behaviors that make this suite of elements particularly interesting for studies on redox oscillations. While Mo and U exhibit a conservative behavior in the ocean (residence time of Mo: ~800 kyr, U: ~400 kyr), a slight surface depletion is observed for V (residence time of V: ~50 kyr). In oxic seawater, their major dissolved species are oxyanions of V(V) (vanadate, HVO_4^{2-}), Mo(VI) (molybdate, MoO_4^{2-}) and U(VI) (uranyl carbonate, $UO_2(CO_3)_3^{4-}$) (Bruland and et al., 1983; Tribovillard et al., 2006).

Vanadate readily adsorbs to Mn and Fe (oxyhydr)oxides in the water column and molybdate is also well known for its strong affinity to particulate Mn (oxyhydr)oxides in oxic settings (Chan and Riley, 1966a,b; Shimmield and Price, 1986; Wehrli and Stumm, 1989; Barling and Anbar, 2004). Moreover, in a recent isotope geochemical study Goldberg et al. (2009) underscored the importance of Fe (oxyhydr)oxides as a solid carrier for Mo to the sediment surface. Upon reductive dissolution of Mn and Fe (oxyhydr)oxides in the surface sediment, V and Mo oxyanions are released into the pore water and either diffuse back into the water column or become trapped by authigenic phases within the sediments (Shaw et al., 1990; Emerson and Huested, 1991; Morford et al., 2005). In reducing (pore) waters V(V) is stepwise reduced to V(IV) and, if free H_2S is present, to V(III) (Wehrli and Stumm, 1989; Wanty and Goldhaber, 1992). Most of the reduced V species are prone to removal from the dissolved phase, through surface adsorption of vanadyl (VO^{2+}) or organic V(IV) complexes, formation of insoluble V(III) oxides or hydroxides and incorporation of V(III) in refractory organic compounds (e.g. porphyrins) or authigenic clay minerals (Breit and Wanty, 1991; Wanty and Goldhaber, 1992; Calvert and Pedersen, 1993). Molybdate undergoes successive sulfidation at H_2S concentrations above a critical threshold level (~0.1 μM; Zheng et al., 2000) leading to the formation of thiomolybdates ($MoO_xS_{4-x}^{2-}$, $1 < x < 4$) (Helz et al., 1996; Erickson and Helz, 2000). Because of the strong affinity of thiomolybdates to reactive surfaces, Mo is readily scavenged in anoxic-sulfidic environments by forming bonds with metal-rich particles (e.g. less reactive Fe oxides), Fe sulfides and sulfur-rich organic molecules (Huerta-Diaz and Morse, 1992; Helz et al., 1996; Bostick et al., 2003; Tribovillard et al., 2004; Vorlicek et al., 2004). If Mo (and presumably also V) is removed from pore water at or directly below the sediment surface, a direct diffusive flux across the benthic boundary may be established (Zheng et al., 2000).

Uranyl carbonate does not adsorb to Mn and Fe (oxy-hydr)oxides or any other inorganic particles in the water column. In reducing pore water, U(VI) is reduced to U(IV), a process that is typically observed in the Fe reduction zone (Barnes and Cochran, 1990, 1991; Klinkhammer and Palmer, 1991; Zheng et al., 2002a). Since U reduction does not occur in the water column of anoxic basins (Anderson et al., 1989a,b), it is believed to be catalyzed by reactive mineral surfaces and, most notably, enzymes produced by Fe and possibly sulfate reducing bacteria (Lovley et al., 1991; Lovley and Phillips, 1992; Lovley et al., 1993; Liger et al., 1999; Zheng et al., 2002a; Suzuki et al., 2005). Reduced U is removed from the pore water through adsorption or precipitation of U oxides (mainly uraninite, UO_2). The resulting concentration gradient promotes a downward diffusive flux of U across the benthic boundary. A variety of interlinked factors have been proposed to control the magnitude of this flux, including the bottom water oxygen concentration, the sinking rate of organic carbon and the combined rates of Fe and sulfate reduction (Zheng et al., 2002a; McManus et al., 2005, 2006; Morford et al., 2009a). It is generally agreed that most of the U in anoxic sediments is delivered by diffusion across the sediment–bottom water interface (McManus et al., 2005; Morford et al., 2009a). Notwithstanding, a few studies have revealed that a significant portion of the U buried in sediments beneath an anoxic water column may be delivered as bioauthigenic U (or particulate non-lithogenic U, PNU) which had originally formed in the photic zone (Anderson et al., 1989a; Zheng et al., 2002a,b). At oxic sites, this organically bound U is completely regenerated during its transit through the water column (Anderson, 1982). According to Zheng et al. (2002b), however, preservation of the bioauthigenic U may reach 100% if water column oxygen concentrations drop below 25 μM.

Once accumulated, trace metals may be re-mobilized if they become temporarily exposed to more oxidizing conditions, e.g. due to re-suspension and bioturbation or bioirrigation. Therefore, sediments underlying oxic bottom water retain only a small fraction of the originally delivered metals (Zheng et al., 2002a; Morford et al., 2009a,b). Because of their different sources (particulate versus diffusive) or diagenetic sinks (oxides, sulfides, association with organic molecules), V, Mo and U are anticipated to respond in different manner to lateral and temporal changes in bottom water oxygenation.

2. STUDY AREA

The coastal area off Peru (Fig. 1) is characterized by southeasterly alongshore winds driven by the Pacific Subtropical Anticyclone throughout most of the year. These atmospheric conditions promote strong offshore Ekman transport of surface waters within the Peru coastal current and upwelling of subsurface waters from the poleward flowing Peru undercurrent (Strub and Montecino, 1998). The upwelled water is oxygen-depleted and rich in nutrients thus enabling a high primary productivity in the photic zone (~3.6 g C m^{-2} d^{-1}; Pennington et al., 2006). Intense degradation of organic matter leads to a near-complete drawdown of dissolved oxygen in the water column. As a result, an OMZ is established above the Peruvian shelf and upper slope extending roughly from <100 to 700 m water depth (oxycline of 22 μM defined by Fuenzalida et al. (2009). While the lower boundary of the OMZ is relatively stable, the upper boundary underlies considerable fluctuations that are mainly tied to the passage of coastal trapped waves (Gutiérrez et al., 2008). These emerge from equatorial Kelvin waves in the equatorial East Pacific and occur more frequently during positive ENSO periods (Brink, 1982; Hormazabal et al., 2001; Pizarro et al., 2001). The propagation of coastal trapped waves is accompanied by a significant thermocline and oxycline deepening, shifting the upper boundary of the OMZ by 100 m water depth or more (Gutiérrez et al., 2008). Most intense oxygenation events have been observed during the El Niño periods of 1982/1983 and 1997/1998 during which the upper boundary of the OMZ deepened to almost 300 m (Levin et al., 2002; Fuenzalida et al., 2009). Seasonal fluctuations are of inferior importance although a maximum in wind speed and coastal upwelling has been reported for austral winter and spring (Scheidegger and Krissek, 1983; Strub and Montecino, 1998; Soto-Mardones et al., 2004).

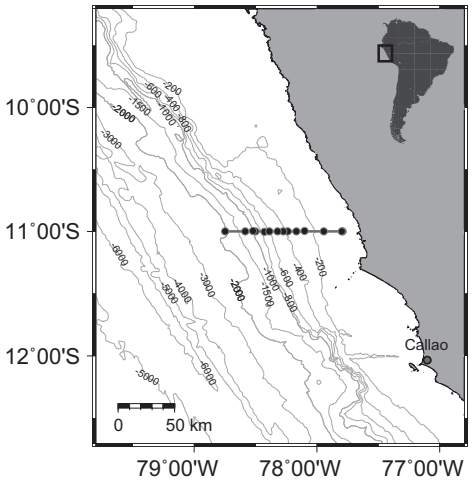

Fig. 1. Location map showing the Peruvian continental margin (bathymetric data from GEBCO 2008 data base). The sampling stations on the 11°S transect (horizontal line) are indicated by the black dots.

Offshore Peru between 10° and 14°S, upwelling-influenced sediments accumulate in a coastal mud lens extending from the depth of the wave base to 500 m water depth on the upper slope. The anomalously fine grained sediments in this area consist of a mixture of terrigenous matter with ~18 wt.% of biogenic silica and organic mater contents of up to 20 wt.% (Scheidegger and Krissek, 1983). Below the mud lens and up to a water depth of >1500 m, strong bottom currents cause reworking and winnowing of sediments leading to a much coarser grain size distribution and lower contents of organic carbon. Furthermore, the high energy regime prevailing mid-slope favors the formation and accumulation of phosphorite crusts and nodules (Reimers and Suess, 1983; Glenn and Arthur, 1988).

Table 1
Geographical coordinates, water depth and water column properties at the sampling stations. Bottom water (BW) temperatures and oxygen concentrations were derived from nearby CTD casts. Sediment data were collected for all MUCs. No pore water data for trace metals are available for MUC52, MUC26 and MUC27.

	Station	Device	Latitude S	Longitude W	Water depth (m)	BW temperature (°C)	BW O_2 (μM)
M77-1	543	MUC52	10°59.99'	77°47.40′	78	12.7	<LD
M77-1	568	BIGO-05	11°00.02′	77°47.72′	85	12.7	<LD
M77-1	470	MUC29	11°00.00′	77°56.61′	145	12.8	<LD
M77-2	016	BIGO-T	10°59.80′	78°05.91′	259	12.0	<LD
M77-1	449	MUC19	11°00.01′	78°09.97′	319	11.1	<LD
M77-1	481	MUC33	78°14.19′	11°00.00′	376	8.3	<LD
M77-1	519	MUC43	78°16.29′	11°00.01′	410	8.3	<LD
M77-1	455	MUC21	11°00.01′	78°19.24′	465	7.9	2.1
M77-1	487	MUC39	11°00.00′	78°23.17′	579	7.2	4.2
M77-1	459	MUC25	11°00.03′	78°25.60′	697	6.1	12.1
M77-1	445	MUC15	10°59.98′	78°30.02′	930	4.8	39.9
M77-1	549	MUC53	10°59.99′	78°31.27′	1005	4.7	41.6
M77-1	460	MUC26	11°00.01′	78°35.11′	1242	3.6	63.8
M77-1	462	MUC27	10°59.97′	78°44.76′	2025	2.3	93.4

<LD: Below limit of detection (~1.5–2.0 μM).

3. MATERIALS AND METHODS

3.1. Sampling and onboard analytics

Fourteen sediment cores were retrieved on a transect along 11°S during the M77-1 and M77-2 cruises of RV Meteor that took place from November 22nd to December 21st of 2008 (Fig. 1). The geographical position and water column properties of all sampling stations are summarized in Table 1. Hydrographic data and oxygen concentrations in the water column were obtained by deploying a CTD/rosette equipped with an oxygen sensor. Sediment samples were retrieved using a video-guided multiple corer (MUC) equipped with PVC liners with an inner diameter of 10 cm. After recovery, MUCs with an undisturbed sediment/bottom water interface were plugged and immediately carried into a cooling lab which was kept at in situ (i.e. seafloor) temperature. The bottom water was siphoned with a plastic tube and filtered through cellulose acetate syringe filters. Sediment subsampling was performed under inert atmosphere in an argon-flushed glove bag. The glove bag was filled and emptied repeatedly in order to remove any oxygen prior to sampling. The MUCs were cut into 1–5 cm thick slices with the highest resolution at the surface and the pore water was separated from the sediment by centrifuging for 20 min at 4500 rpm. The centrifuge vials were then transferred into a second glove bag where the supernatant water was filtered through cellulose acetate syringe filters. A small pore water aliquot was acidified in the glove bag with ascorbic acid for onboard Fe analyses. Concentrations of ferrous Fe and H_2S were determined shortly after pore water recovery by standard spectrophotometric techniques (Stookey, 1970; Grasshoff et al., 2002). Subsamples for metal analyses were stored in acid-cleaned LDPE vials and acidified with concentrated HNO_3 (supra pure). The residual sediments in centrifuge vials were frozen and stored for total digestions after the cruise. An additional sediment aliquot was taken from a parallel MUC and stored in air tight plastic cups for the determination of water content and porosity as well as for total organic carbon (TOC) and total sulfur (TS) analyses. Two of the sediment cores discussed in this article were obtained from benthic lander deployments (Biogeochemical Observatory – BIGO; Sommer et al., 2006). These cores were processed in the same way as described above for MUCs.

3.2. Chemical analyses

The TOC and TS content of freeze-dried and ground sediment samples was determined by flash combustion in a Carbo Erba Element Analyzer (NA1500) with an analytical precision of about 1% for replicate analyses. For total metal concentrations, 100 mg of freeze dried and ground sediment sample were digested in HF (40%, supra pure), HNO_3 (65%, supra pure) and $HClO_4$ (60%, p.a.). The accuracy of the digestion procedure was monitored by including method blanks and the reference standards SDO-1 (Devonian Ohio Shale, USGS; Govindaraju, 1994), MESS-3 (Marine Sediment Reference Material, Canadian Research Council) as well as the in-house standard OMZ-1. Average values of replicate digestions were generally well within the recommended ranges with relative standard deviations (RSD) being <1% for Al, Mn and Fe and <5% for V, Mo and U ($n = 9$).

The analysis of Mn, Fe and Al in digestion solutions was carried out using an inductively coupled plasma optical emission spectrometer (ICP-OES, VARIAN 720-ES). Trace metal concentrations (V, Mo and U) in digestion solutions as well as the metal concentration (Mn, Fe, V, Mo and U) of all bottom and pore water samples were measured by inductively coupled plasma mass spectrometry (ICP-MS, Agilent Technologies 7500 Series) in H_2 reaction (Fe) or He collision (other elements) mode. Samples were diluted 20-fold with 2% HNO_3 (sub-boiled, distilled) prior to analysis. Calibration standards for bottom and pore water analyses were prepared with an appropriate volume of artificial seawater in order to adjust them to the sample matrix. Samples and standards were spiked with an internal standard solution (Sc, Y and In) in order to correct for instrumental mass bias. Despite internal standardization, an instrumental drift was observed for U. Therefore, each block of four

Table 2
Accuracy values for replicate measurements of CASS-5 Nearshore Seawater Reference Material ($n = 87$). The measured values are average concentrations ± standard deviation (% RSD).

Element	Measured value (nM)	Certified value (nM)
Mn	47.0 ± 2.5 (5.4%)	47.7 ± 3.6
Fe	<LD	25.8 ± 2.0
V	24.3 ± 2.3 (9.3%)	25.9 ± 2.7
Mo	95.4 ± 1.5 (1.6%)	102[a]
U	12.1 ± 0.3 (2.3%)	12.6[a]

<LD: below limit of detection.
[a] Recommended value without certification.

samples was bracketed with a pair of an appropriate calibration standard and a certified reference standard (CASS-5, Nearshore Seawater; Canadian Research Council) was measured in the middle of each block. The drift was corrected for by calculating a drift factor from the change in U concentration measured for the calibration standard and the goodness of the correction was monitored by comparing the concentration measured for the reference standard with the certified value. Accuracies for replicate analyses of CASS-5 are summarized in Table 2. Our results for Mn and V are in good agreement with the certified ranges and precision values based on replicate measurement of CASS-5 and pore water samples are <10% RSD for all elements. CASS-5 is not certified for Mo and U but the deviation of our average values from the recommended values are <10% which is a typical uncertainty for trace metals in reference standards. Concentrations of Fe in CASS-5 are below the detection limit of our method. However, the ICP-MS results for total Fe are mostly in good agreement with the ferrous Fe data obtained onboard by spectrophotometry. Deviations >5% occur mainly at the OMZ boundaries and are therefore attributed to higher concentrations of ferric Fe. Diffusive benthic fluxes for Fe reported in later sections and all pore water Fe plots are based on the onboard Fe data.

3.3. Quantification of trace metal accumulation

Sediment mass accumulation rates (MARs; in $g\,cm^{-2}\,kyr^{-1}$) were calculated from sedimentation rate (SR; in $cm\,kyr^{-1}$), dry bulk density (ρ_{dry}; in $g\,cm^{-3}$) and the average porosity at the lower core end (ϕ_∞):

$$MAR = \rho_{dry}(1-\phi_\infty)SR$$

Sedimentation rates were obtained for selected cores by measuring gamma-ray excess ^{210}Pb activities and modeling the resulting profiles as described in Meysman et al. (2005). Porosity values were determined from the water loss after freeze drying and dry bulk density was approximated from TOC concentrations using an empirical relationship that is based on data for Peru upwelling sediments from Böning et al. (2004). Multiplying the MAR with the average authigenic metal concentration ($[Me]_{auth}$) yields the authigenic metal MAR. The authigenic metal concentration, which is defined as the difference between the total metal concentration ($[Me]_{tot}$) and the detrital background ($[Me]_{detr}$), was calculated as follows:

Table 3
Metal/Al ratios for average andesite in the Andean Arc and common reference materials.

Metal/Al	Andesite in the Andean Arc[a]	Post-Archean average shale[b]	Average upper continental crust[c]
Fe/Al	0.47	0.56	0.44
Mn/Al ($\times10^{-2}$)	1.23	0.95	0.75
V/Al ($\times10^{-3}$)	1.39	1.44	1.33
Mo/Al ($\times10^{-4}$)	0.26	0.15	0.19
U/Al ($\times10^{-4}$)	0.37	0.32	0.35

[a] GEOROC data base, Max-Planck Institute for Chemistry, Mainz, Germany (Sarbas and Nohl, 2009).
[b] Taylor and McLennan (1985).
[c] McLennan (2001).

$$[Me]_{auth} = [Me]_{tot} - \frac{[Me]_{detr}}{[Al]_{detr}}[Al]_{tot} \quad (1)$$

Böning et al. (2004) demonstrated that the chemical composition of andesite is an appropriate representation of the detrital background on the Peruvian margin. Average metal/Al ratios for andesite rocks in the Andean Arc were derived from the GEOROC data base of the Max-Planck Institute for Chemistry, Mainz, Germany (Sarbas and Nohl, 2009). A comparison between the ratios of andesite in the Andean Arc, Post-Archaean Australian average shale and average upper continental crust is provided in Table 3.

Diffusive fluxes of metals across the benthic boundary were calculated by Fick's first law of diffusion:

$$\text{Flux} = -\phi D_{sed}\frac{d[C]}{dx} \quad (2)$$

where $d[C]/dx$ denotes the concentration difference between the bottom water and the uppermost pore water sample divided by the depth of the uppermost pore water sample (0.5 cm). By definition, positive fluxes are directed into the sediment. Diffusion coefficients for metal ions in seawater (D_{sw}) were adjusted to in situ temperature and pressure using the Stokes–Einstein equation. Diffusion coefficients for sediments (D_{sed}) were calculated as:

$$D_{sed} = \frac{D_{sw}}{\theta^2} \quad (3)$$

and tortuosity (θ^2) was derived from porosity using the following relationship from Boudreau (1996):

$$\theta^2 = 1 - \ln(\phi^2) \quad (4)$$

Diffusion coefficients for Fe, Mn, Mo (MoO_4^{2-}) and U (UO_2^{2+}) under standard conditions were taken from Li and Gregory (1974), Morford et al. (2009a) pointed out that the D_{sw} of Mo would be more appropriate for calculating diffusive fluxes for $UO_2(CO_3)_3^{4-}$, the major U species in seawater. However, in order to ensure consistency with most other studies on the diagenetic behavior of U, we decided to adhere to the D_{sw} of UO_2^{2+}. Because of an apparent lack of a published D_{sw} for V, we adopted the one of Mo (MoO_4^{2-}) (cf. Emerson and Huested, 1991), which appears to be reasonable considering that oxyanions are the major V species in seawater (see Section 1.2).

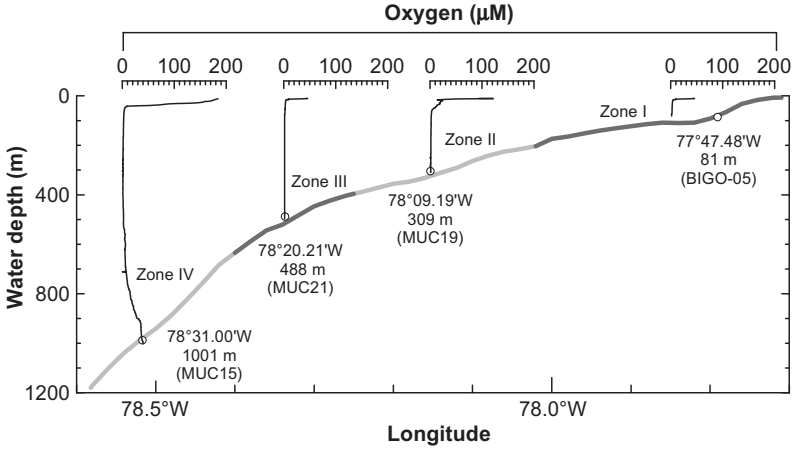

Fig. 2. Bathymetry (data from GEBCO 2008 database) and concentration-depth profiles for dissolved oxygen at selected CTD stations on the 11°S transect. The alternating shades of gray of the bathymetry represent zones I to IV in Fig. 3. Circles depict the exact location of the CTD casts. The sediment core closest to each station is given in parentheses.

4. RESULTS AND DISCUSSION

4.1. Sediment redox state and diagenetic zoning

At the time of sampling, the Peruvian margin was overlain by a pronounced OMZ with the core ($O_2 < 2$ µM) ranging roughly from 50 to 500 m water depth (Fig. 2). Pore water profiles of Mn, Fe, H_2S, U, V and Mo are shown in Fig. 3. The stations are ordered according to increasing water depth and combined in 4 subpanels based on similarities in the shape of their pore water profiles. These subpanels and the corresponding areas on the margin (i.e. water column and sediments) will be referred to as zone I (shallowest stations) to zone IV (stations below ~600 m water depth) in the following sections. Fig. 2 shows exemplary oxygen profiles in the water column for each of the four zones. The only zone where bottom water oxygen concentrations rose above a few µM during the sampling campaign is zone IV.

Highest dissolved Mn and Fe concentrations (up to 190 nM of Mn and 35 µM of Fe) are observed in zone I where pore water profiles of Mn and Fe display pronounced maxima close to the sediment/bottom water interface. Lower concentrations and less steep concentration-depth gradients prevail in zones II and III. In zone IV, the uppermost few cm of the sediments show again a surface maximum in Mn whereas the Fe concentrations drop to zero. Diffusive benthic fluxes for Mn, Fe, U, V and Mo are shown in Table 4 and plotted against water depth in Fig. 4. Highest flux values for both Mn and Fe are observed in the shallowest core in zone I (BIGO-05). The Mn fluxes decrease steadily with increasing water depth to values close to zero in MUC21 (465 m) and increase again below. The Fe fluxes are more randomly distributed in zones II and III and are zero in zone IV.

The Mn and Fe flux across the benthic boundary is driven by reductive dissolution of reactive Mn and Fe (oxyhydr)oxides in the surface sediments (Froelich et al., 1979; Burdige, 1993; Pakhomova et al., 2007). Notwithstanding, most of the Mn which is delivered to the OMZ is already reduced in the water column (cp. Böning et al., 2004). This is illustrated by low pore water Mn concentrations and diffusive fluxes compared to other continental margin settings (Figs. 3 and 4; cp. Pakhomova et al., 2007 and references therein), little downcore variability of Mn/Al in the sediments (see Supplementary EA-Table 1 in the Electronic Annex) and a strong depletion of Mn with respect to the detrital background in sediments on the entire continental margin (Fig. 5 and Böning et al., 2004). Some Fe reduction might occur in the water column as well. However, the benthic Fe fluxes reported here fall in the upper range of values reported for a wide range of environments (Severmann et al., 2010; Noffke et al., 2011), suggesting that the surface sediments are the principal locus of Fe reduction in the Peruvian OMZ. A similar conclusion has been drawn by Bruland et al. (2005) based on the distribution of dissolved ferrous Fe in the water column. The magnitude of the diffusive Fe flux across the sediment/bottom water interface is controlled by both the bottom water oxygen concentrations and the availability of reactive Fe (Pakhomova et al., 2007; Severmann et al., 2010). Assuming that the bottom water oxygen level remains favorable for the transfer of ferrous Fe across the benthic boundary for a prolonged period of time, the reactive Fe pool will become progressively depleted, unless it is replenished through detrital input. Such a scenario of reactive Fe depletion in sediments underlying a permanently anoxic but non-sulfidic water column is in agreement with Fe/Al ratios significantly below the detrital background in zones II and III (Fig. 5) and low concentrations of reactive Fe minerals in the central part of the OMZ reported by Suits and Arthur (2000). Apparently, detrital inputs from the continent are not sufficient to balance the reductive loss of Fe from sediments in this section of the Peruvian margin. Some of the released Fe seems to be laterally transported in the water column and re-oxidized and deposited at the oxycline in zone IV (~900–1100 m) where Fe/Al ratios increase above the detrital background (Fig. 5). Here, elevated bottom water oxygen levels (~40 µM, Table 2 and Fig. 2) prevent the Fe which is reduced in the sediments from being transported across the benthic boundary (Fig. 3). Therefore,

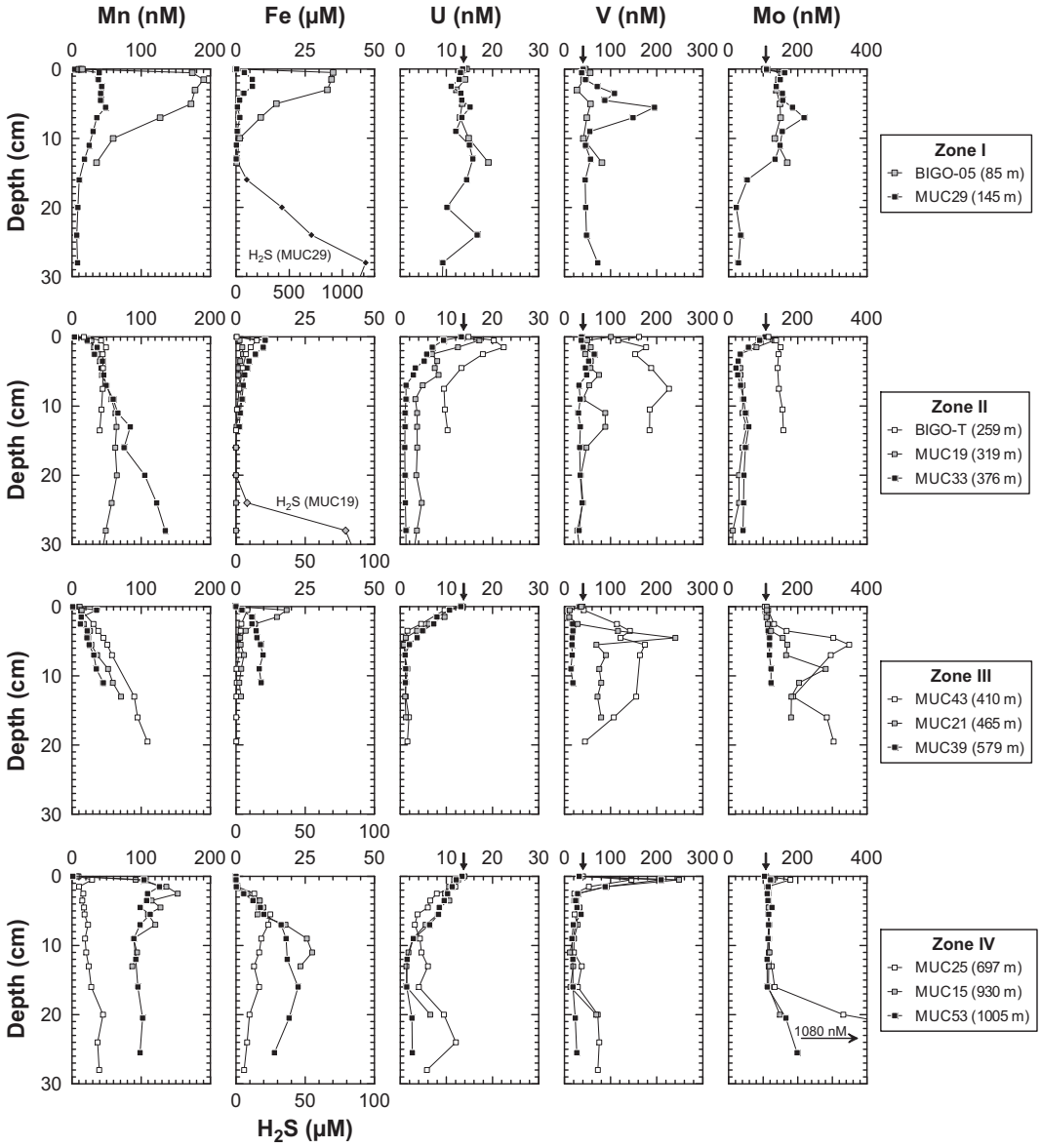

Fig. 3. Pore water profiles for Mn, Fe, H_2S, U, V and Mo. Concentrations of Fe and H_2S (diamonds) are shown in common diagrams. The only stations where H_2S concentrations were found to be above the detection limit of the method applied (~2 μM) are MUC29 and MUC19. The uppermost data point of each profile (depth of zero) represents bottom water concentrations. Arrows above upper *x*-axis indicate average seawater values ($[U]_{sw} = 13.7$ nM, $[V]_{sw} = 40.3$ nM, $[Mo]_{sw} = 108$ nM).

most of the delivered excess Fe may be retained in the sediments. A similar export mechanism of reactive Fe has been reported for sediments of the Arabian and Mexican upwelling areas where sedimentary Fe/Al ratios are significantly higher below than within the OMZ (Van der Weijden et al., 1999; Nameroff et al., 2002). In analogy to Fe, increasing pore water Mn concentrations (Fig. 3) and diffusive benthic fluxes (Fig. 4) below zone III could imply a relative enrichment of Mn at the sediment surface in zone IV. However, because of its shallower reduction zone and sluggish oxidation kinetics compared to Fe, most of the Mn which is liberated at the sediment surface may diffuse back into the water column. As a consequence of this shallow recycling, any delivery of 'excess' Mn in zone IV is not recorded in the Mn/Al ratios (Fig. 5).

The relatively high benthic Fe fluxes observed at the shallowest station (BIGO-05) may partly be due to an increased supply of detrital (oxyhydr)oxides from the continent (Suits and Arthur, 2000). Another portion of the pore water Fe at the shelf stations, however, has likely been delivered from zones II and III through lateral transport of dissolved Fe in the water column and re-oxidation and deposition at the upper oxycline during periods of shelf oxygenation. Upon the recurrence of anoxic conditions (like those prevailing during our sampling campaign), this pool of excess Fe is reduced and partly recycled into the water column, thus leading to particularly high benthic fluxes compared to stations in zones II and III. A similar alternation of particulate supply and reductive release may be anticipated for Mn which shows also higher pore

Table 4
Diffusive flux of Mn, Fe, U, V and Mo across the sediment/bottom water interface. Positive values denote a downward flux into the sediment.

Core	Water depth (m)	Diffusive benthic flux				
		Mn (nmol cm^{-2} yr^{-1})	Fe (μmol cm^{-2} yr^{-1})	U (nmol cm^{-2} yr^{-1})	V (nmol cm^{-2} yr^{-1})	Mo (nmol cm^{-2} yr^{-1})
BIGO-05	85	−40.6	−8.83	+0.13	−4.5	−16.7
MUC29	145	−9.3	−0.66	+0.08	+1.3	−19.7
BIGO-T	259	−6.5	−1.89	−0.90	+17.2	−8.3
MUC19	319	−5.7	−0.33	−0.64	+18.7	−8.6
MUC33	376	−4.0	−2.30	+0.53	+0.1	+4.9
MUC43	410	−2.2	−0.85	+0.52	−0.8	−2.9
MUC21	465	−0.5	−3.19	+0.31	+6.2	−0.1
MUC39	579	−6.9	−0.43	+0.30	+6.1	−1.3
MUC25	697	−3.1	0	+0.10	−24.1	−16.1
MUC15	930	−12.5	0	+0.20	−45.6	−4.6
MUC53	1005	−13.1	0	+0.10	−32.6	−3.2

water concentrations and diffusive benthic fluxes in zone I compared to zones II and III. As Mn/Al ratios in zone I are similarly low as in the other zones (Fig. 5), it is anticipated that accumulation of Mn during oxic periods and release during anoxic periods largely cancel out each other. In contrast, the Fe/Al ratios are equal to or slightly above the detrital background in zone I suggesting a more efficient trapping of the reactive Fe which is delivered from land and the OMZ during periods of shelf oxygenation. This is in agreement with results from Suits and Arthur (2000) who reported the highest degrees of pyritization (DOPs) and the highest pyrite concentrations on the entire Peruvian margin for sediments on the shelf.

The above discussion of Mn and Fe data reveals a complex interplay between reductive release, lateral transport, deposition and recycling across the margin. This framework of how redox gradients and oscillations affect metal cycling in the Peruvian OMZ will be revisited and substantiated in the following discussion of U, V and Mo data.

4.2. Controls on the benthic flux of trace metals

4.2.1. Uranium

Most sediment cores in zone II to zone IV show dissolved U concentrations decreasing downward from seawater-like values at the top to 1.0–3.0 nM at 5–10 cm below surface (Fig. 3). At greater sediment depth, U concentrations remain either constant or increase again in MUC15 and MUC53. In agreement with previous studies on anoxic marine sediments, the removal of U close to the sediment surface is attributed to reduction of U(VI) to U(IV) followed by precipitation of UO_2 or other authigenic U phases (e.g. Barnes and Cochran, 1990, 1991; Klinkhammer and Palmer, 1991). The resulting downward diffusive U flux increases between zone IV and zone II and reaches its highest value in MUC33 at 376 m (Table 4, Fig. 4). Previous studies in a broad range of oxic and hypoxic marine settings revealed striking relationships between authigenic U accumulation and the organic carbon rain and degradation rates as well as the oxygen penetration depth (Zheng et al., 2002a; McManus et al., 2005; Morford et al., 2009a). All of these parameters dictate the extent of reducing conditions in the surface sediments and, therefore, the activity of Fe and sulfate reducing bacteria, both of which are capable of mediating U reduction (Lovley et al., 1991; Lovley and Phillips, 1992; Zheng et al., 2002a). During our sampling campaign, the Peru margin was characterized by a continuous landward decrease in bottom water oxygen concentration (Table 1, Fig. 2) and increasing carbon rain and degradation rates as well as Fe and sulfate reduction rates towards the shore (Bohlen et al., 2011). Furthermore, U depletion occurred generally at or shortly below the depth of the highest Fe concentrations (Fig. 3). These observations support the general conception that authigenic U accumulation is controlled by the combined rates of Fe and sulfate reduction close to the sediment/bottom water interface (Zheng et al., 2002a; McManus et al., 2005).

At depths shallower than MUC33, surface sediments are still favorable for U reduction, which is demonstrated by maxima in dissolved Fe at 0.5 cm and bottom water oxygen concentrations close to zero. However, dissolved U concentrations above bottom water values at the sediment surface of MUC19 and particularly BIGO-T (Fig. 3) indicate a considerable diffusive U flux out of the sediments (Table 4, Fig. 4). Furthermore, pore water U profiles in zone I do not show any regular U depletion but scatter around bottom water values. Similar U profiles have been observed in bioturbated and/or bioirrigated sediments underlying oxic bottom water (Zheng et al., 2002a; Morford et al., 2009a,b) or in estuaries with seasonal oxygen fluctuations in the water column (Shaw et al., 1994). In such settings, authigenic U which had precipitated during more reducing periods undergoes transient re-oxidation and recycling through diffusion across the benthic boundary. Pore water U in zone I follows a highly transient zig–zag-pattern which may be ascribed to ENSO-related high amplitude changes between oxic and anoxic conditions. In contrast to that, the dissolved U distribution in MUC19 is much closer to steady state with respect to the present bottom water oxygen level (cf. MUC33). Accordingly, the continuous growth of the surficial U peak between >320 and ~250 m (MUC19, BIGO-T) and the absence of any pore water U depletion in zone I are attributed to the enhanced intensity, frequency and duration of oxygenation episodes with decreasing water depth (Gutiérrez et al., 2008).

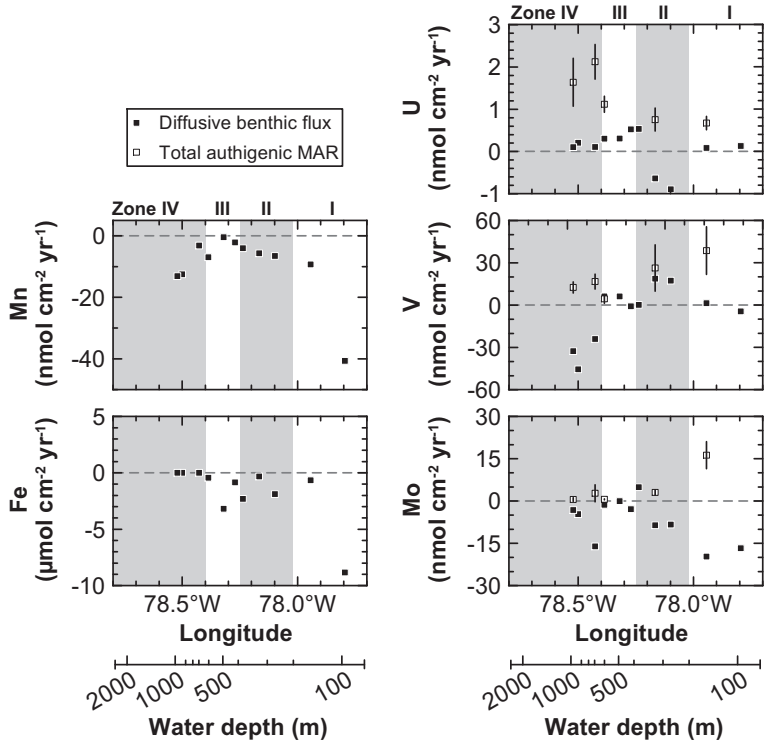

Fig. 4. Plots of diffusive benthic fluxes (Mn, Fe, V, Mo and U) for all cores where pore water data are available and authigenic MARs for selected cores (U, V and Mo) against longitude. An alternative scale bar translating longitude into water depth is shown as well. The exact values and error margins are listed in Tables 4 and 5. Positive diffusive fluxes are directed downward into the sediment. Horizontal dashed lines depict a diffusive flux or MAR of zero. The grayish and whitish arrays represent zones I to IV in Fig. 3.

Zheng et al. (2002a) reported a threshold oxygen level of 15 µM above which U remobilization may occur. However, Levin et al. (2002) pointed out that even during the intense El Niño event of 1997/1998 the bottom water oxygen concentration at the deepest station where U remobilization is observed (MUC19) did not rise above ~2.2 µM. Although the Peruvian margin experienced several positive ENSO periods in the years prior to our sampling campaign, there was no major El Niño event comparable to those of 1982/1983 and 1997/1998 (see Fig. A1 Appendix A for a time series of the Oceanic Niño Index, ONI). We therefore assume that even a minute increase in bottom water oxygen concentration (i.e. $\leqslant$2 µM), shifting the U(VI)/U(IV) boundary by a few cm, may be sufficient to cause shallow remobilization of authigenic U. The shift of the redox boundary is likely supported by reduced fluxes of particulate organic carbon from the overlying water column during positive ENSO periods (Gutiérrez et al., 2000). Another factor that potentially enhances U remobilization is the activity of bioturbating organisms. Levin et al. (2002) and Gutiérrez et al. (2008) demonstrated that bioturbating fauna rapidly inhabits the Peruvian shelf and upper slope sediments during oxygenation episodes and even persists for several months after anoxic conditions have reestablished.

4.2.2. Vanadium and molybdenum

It has been argued in previous studies that downward diffusion of V and Mo across the sediment/bottom water interface due to authigenic removal is the primary mechanism of V and Mo accumulation in sediments on the Peruvian margin and other upwelling areas (Zheng et al., 2000; Böning et al., 2004, 2009). A downward directed concentration gradient across the sediment surface requires a shallow authigenic V and Mo sink. This sink must be highly effective to prevent any excess V and Mo that is released from Mn and Fe (oxyhydr)oxides from accumulating in pore water. Otherwise a shallow peak will establish promoting both an upward directed diffusive flux across the benthic boundary and a downward flux towards the authigenic sink.

Most sediment cores in zones I to IV display dissolved V and Mo concentrations above local bottom water values in the uppermost section of the sediment column (~0–10 cm; Fig. 3). Some of these shallow peaks coincide with maxima in dissolved Mn and Fe suggesting a common supply or cycling of V and Mo with Mn and/or Fe. This is particularly the case in zone IV where both V and Mo display pronounced peaks in the Mn reduction zone (up to 248 nM of V and 179 nM of Mo). However, dissolution of Mn (oxyhydr)oxides alone is unlikely to account for the shallow V and Mo enrichment in pore water since diffusive benthic Mn fluxes range in the same order of magnitude as the diffusive V and Mo fluxes (Table 4, Fig. 4). For comparison, in other settings where release of V and Mo from Mn (oxyhydr)oxides has been postulated, dissolved Mn concentrations in pore water (and by inference the diffusive benthic fluxes) exceed those of V and Mo by several orders of magnitudes (Shaw et al., 1990; Morford et al., 2005).

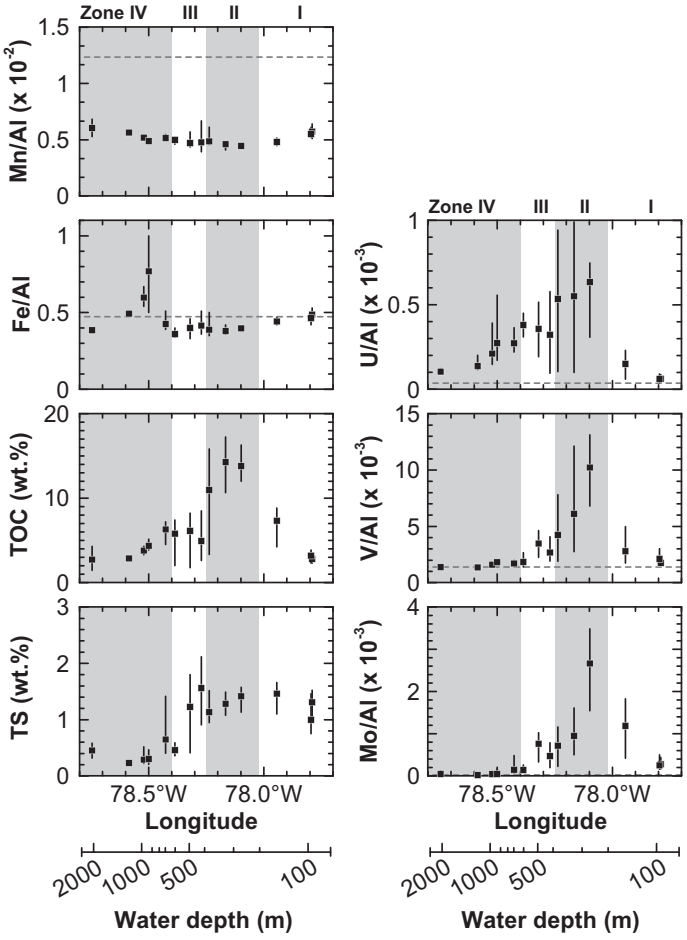

Fig. 5. Average Mn/Al, Fe/Al, TOC, TS, U/Al, V/Al and Mo/Al ratios for each core plotted against longitude. An alternative scale bar translating longitude into water depth is shown as well. Normalized metal concentrations are used to eliminate the effect of varying dilution with detrital material. Error bars span the range between the highest and lowest value of each core. Horizontal dashed lines depict the metal/Al ratio of the detrital background (andesite in the Andean Arc, see Table 2). The grayish and whitish arrays represent zone I to zone IV in Fig. 3. Solid phase geochemical data are summarized in Supplementary EA-Table 1 and EA-Table 2 in the Electronic Annex.

Surface sediments in zone IV receive high loads of reactive Fe that has been supplied from zones II and III through lateral transport within the anoxic water column and re-precipitation at the lower boundary of the OMZ (cf. Section 4.1). However, since the regeneration of V and Mo occurs at shallower sediment depth than Fe reduction, release during quantitative dissolution of Fe (oxyhydr)oxides cannot account for the surficial V and Mo peaks either. In fact, the coinciding zones of V, Mo and Fe removal at 2–3 cm do rather suggest that most of the V and some of the Mo released at the sediment surface is re-adsorbed to Fe (oxyhydr)oxides shortly below. Another possible explanation for the shallow V and Mo accumulation in pore waters of zone IV is release form fragile organic substances in the thin oxic surface layer (Brumsack and Gieskes, 1983; Audry et al., 2006). Neither of the above explanations can be verified based on our data. However, since both V and Mo are attracted by metallic surfaces under oxic conditions (e.g. Chan and Riley, 1966a,b; Barling and Anbar, 2004; Goldberg et al., 2009) and since they are both liberated concomitantly with Mn we anticipate that some kind of particulate shuttle is involved. Below the shallow peaks, the presence of dissolved Fe and seawater-like V and Mo concentrations indicate that H_2S concentrations in pore waters of zone IV are too low as to drive significant V reduction or Mo sulfidation. As a consequence, most of the liberated V and Mo is lost through diffusion across the benthic boundary (see negative benthic fluxes in Table 4 and Fig. 4). Again increasing concentrations below 15 cm indicate ongoing mobilization of V and Mo (and also U) below the depth of Mn and Fe recycling. This could be related to deep-reaching bioturbation and/or bioirrigation causing re-oxidation of authigenic metal phases that were precipitated during more reducing periods or at greater sediment depth (Morford et al., 2009b). This explanation is supported by findings of Levin et al. (2002) who reported a comparably high abundance of burrowing fauna below the permanent OMZ.

Pore water profiles in zone I and the shallowest core in zone II (BIGO-T) display somewhat erratic V and Mo peaks both within and below the Mn and Fe reduction zones. Release from either Mn or Fe (oxyhydr)oxides can-

not be distinguished at the given sampling resolution. However, the coincident Mn, Fe and Mo increase in the uppermost cm (Fig. 3) and the high upward diffusive Mn, Fe and Mo fluxes (Table 4, Fig. 4) in zone I suggest some Mo release from dissolving (oxyhydr)oxides. The lack of a significant benthic V flux might be related to shallow re-adsorption of V(IV) species that are known to form in manganous or ferruginous pore waters (e.g. Calvert and Pedersen, 1993). Below the Mn and Fe reduction zone and up to a depth of ~10 cm, pore water profiles of V and Mo display a similar zig–zag-pattern as the U profiles. These transient irregularities indicate that V and Mo are also affected by remobilization during periods of shelf oxygenation. The pore water Mo profile of MUC29 in zone I shows a steep decrease below 13 cm which is coincident with the accumulation of H_2S (Fig. 3). This is in excellent agreement with the general conception of Mo being scavenged from pore water at a critical threshold concentration of H_2S (Helz et al., 1996; Erickson and Helz, 2000; Zheng et al., 2000). Intense Mo authigenesis close to the sediment surface would theoretically support a downward diffusive Mo flux across the benthic boundary. However, because of the shallow accumulation of dissolved Mo from metal (oxyhydr)oxides and re-dissolved authigenic phases, the actual benthic flux in MUC29 is directed out of the sediment (Table 4 and Fig. 4).

At greater depth than BIGO-T, re-oxidation occurs less frequently, which should favor shallow Mo authigenesis and diffusive resupply from the bottom water. Both MUC19 and MUC33 in zone II display sharp concentration gradients at or shortly below the sediment surface and a Mo minimum at shallow depth (<30 nM at 3–5 cm; Fig. 3). We did not detect any shallow H_2S in MUC19 and MUC33. However, the threshold level for sulfidation of molybdate and Mo–Fe–S co-precipitation reported by Zheng et al. (2000) is clearly below the detection limit of our H_2S method (~2 μM). Therefore, active Mo authigenesis might have occurred at the time of sampling. Both MUC19 and MUC33 display TOC maxima at 3 to 7 cm depth (see Supplementary EA-Table 2 in the Electronic Annex) suggesting that hot spots of H_2S production are associated with organic-rich micro niches. MUC33 is the only core where a significant downward benthic Mo flux was observed in this study (Table 4). In this permanently anoxic area of the Peruvian margin, the development of a downward decreasing Mo gradient across the benthic boundary is likely favored by the continuous stripping of Mn and Fe in the water column and the surface sediments, respectively (see Section 4.1). Because of the strong Mn and Fe depletion arising from that (Fig. 5), sediment particles provide little adsorption sites for Mo which would then impede the downward benthic flux upon its release during early sediment diagenesis.

Pore water profiles of V and Mo in zone III are more heterogeneous and generally somewhat scattered. This is commonly observed in continental margin sediments (e.g. Shaw et al., 1990; Morford et al., 2005) and has been assigned to H_2S production in microenvironments (Zheng et al., 2000) and the contrasting solubility of V and Mo species in manganous or ferruginous versus sulfidic pore waters (Calvert and Pedersen, 1993; Algeo and Maynard, 2004). Furthermore, zone III is located at the transition between the permanently anoxic and the hypoxic section of the Peruvian margin (Table 1, Fig. 2). Although fluctuations in bottom water oxygenation are less frequent and vigorous here compared to zone I, non-steady state diagenesis might have contributed to the irregular shape of the pore water profiles. The negative excursions in the Mo profiles of zone III may indicate some Mo authigenesis in distinct depth intervals. However, Mo concentrations are always ⩾bottom water values suggesting that pore waters are generally not sulfidic enough as to support an appreciable downward benthic Mo flux. Authigenic removal of V(IV) may also take place under non-sulfidic conditions (e.g. Calvert and Pedersen, 1993), which could explain the downward benthic V flux in MUC21 and MUC39 (Table 4).

In summary, the pore water V and Mo data suggest that direct diffusive supply of V and particularly Mo is limited to sediments in a narrow depth range underlying the most persistent and pronounced OMZ (~ > 320–400 m). In the other areas, V and Mo are rather delivered with solid carriers such as detrital particles whose surfaces are coated with metallic (oxyhydr)oxides. Strictly speaking, this interpretation is only valid for the exact time of our sampling campaign. However, the sampling was conducted following a 1-year-lasting negative ENSO period (see Fig. A1 Appendix A) and during the season of most intense upwelling (e.g. Scheidegger and Krissek, 1983). It is unlikely, that conditions are much more favorable for diffusive V and Mo supply during other, presumably more oxic periods.

4.3. Long-term accumulation of trace metals

All of the three trace elements investigated show highest Al-normalized concentrations in zone II, coincident with the TOC maximum (Fig. 5). At greater water depth, V and Mo concentrations drop rapidly to the detrital background whereas U concentrations remain elevated on the entire continental margin. The opposite is observed on the shelf, where U and V concentrations drop abruptly at depth ⩽ BIGO-T whereas Mo concentrations decrease more gradually. These patterns are generally in good agreement with previously published data for the Peruvian upwelling area (Böning et al., 2004).

Table 5 shows a compilation SRs, MARs and authigenic metal MARs for selected cores (see Supplementary EA-Fig. 1 in the Electronic Annex for profiles of excess ^{210}Pb and model fits). Dividing the SRs by the length of the respective cores reveals that the study intervals cover a time span of approximately 300 (MUC29) to 1000 (MUC19) yr. A comparison of diffusive benthic U, V and Mo fluxes with authigenic MARs is provided in Fig. 4. The above defined depth range, encompassing the most persistent and pronounced OMZ (~ > 320–400 m or 78.15–78.25°W), is the only area where the diffusive supply of all trace metals investigated is broadly in agreement with their total authigenic MARs (extrapolating the authigenic MAR of MUC19 to the neighboring core MUC33). In the remaining areas, the lack of agreement between these two calculated

Table 5
Compilation of sedimentation rates (SR), mass accumulation rates (MARs) and authigenic metal MARs for selected cores. See Supplementary EA-Fig. 1 in the Electronic Annex for profiles of excess ^{210}Pb and model fits.

Core	Water depth (m)	SR (cm kyr^{-1})	ϕ_∞	ρ_{dry} (g cm^{-3})[b]	MAR (g cm^{-2} kyr^{-1})	Authigenic metal concentration[c]			Authigenic metal MAR		
						$[U]_{auth}$ (nmol g^{-1})	$[V]_{auth}$ (nmol g^{-1})	$[Mo]_{auth}$ (nmol g^{-1})	U (nmol cm^{-2} yr^{-1})	V (nmol cm^{-2} yr^{-1})	Mo (nmol cm^{-2} yr^{-1})
MUC29	145	160[a]			28[a]	23 ± 6	1275 ± 604	580 ± 170	0.65 ± 0.16	36 ± 17	16.2 ± 4.8
MUC19	319	50	0.89	1.54	8	89 ± 32	3033 ± 1937	363 ± 114	0.75 ± 0.27	26 ± 16	3.1 ± 1.0
MUC39	579	26	0.70	2.27	18	63 ± 11	170 ± 174	34 ± 9	1.11 ± 0.19	3.0 ± 3.1	0.60 ± 0.16
MUC25	697	81	0.70	2.18	53	39 ± 8	252 ± 101	51 ± 57	2.08 ± 0.41	13 ± 5	2.7 ± 3.0
MUC53	1005	58	0.63	2.38	51	31 ± 11	175 ± 77	7 ± 12	1.60 ± 0.56	9 ± 4	0.35 ± 0.61

[a] Approximate SR and MAR derived from Reimers and Suess (1983).
[b] Dry bulk density was estimated from TOC using an empirical relationship that is based on data for Peru upwelling sediments from Böning et al. (2004): $\rho_{dry} = -0.08[TOC] + 2.68$ ($R^2 = 0.70$, $n = 16$).
[c] Given as mean value ± SD.

parameters could reflect temporal variability in pore water chemistry. However, as ENSO conditions were negative during the 12 months preceding our sampling campaign, it may be anticipated that redox conditions on the Peruvian margin were rather favorable for diffusive V and Mo supply (see Fig. A1 Appendix A and previous section). This, along with the striking mismatch between the highest U MARs (zone IV) and the location of the permanent OMZ, suggests that mechanisms other than diffusion across the benthic boundary should be considered for trace metal supply and/or accumulation in the remaining areas.

4.3.1. Solid phase speciation of uranium

Authigenic U MARs in zone IV exceed the corresponding benthic fluxes by a factor of up to 20 and are higher than any of the benthic fluxes hitherto reported for anoxic marine sediments (up to 1.52 nmol cm^{-2} yr^{-1} in the California Borderland Basins; Zheng et al., 2002a). The only known additional source of authigenic U to marine sediments is particulate non-lithogenic U (PNU) in sinking organic matter (Anderson et al., 1989a; Zheng et al., 2002a,b). Preservation of PNU is favored by the persistent anoxia in the Peruvian OMZ (Zheng et al., 2002b). Moreover, the distribution of U/Al ratios and TOC concentrations across the margin is highly correlated (Fig. 5, $R^2 = 0.79$, $n = 148$) suggesting that organic matter plays more than an indirect role for the authigenic accumulation of U. The plausibility of PNU as an important U source to the sediment may be evaluated by comparing the U/TOC ratios of water column particulate matter and surface sediments. Unfortunately, we do not dispose of U/TOC ratios for particulate matter off Peru. Zheng et al. (2002) reported U/TOC ratios of 0.33–0.45 × 10^{-4} for water column particulate matter in the NE Pacific, offshore California. The U/TOC ratios of surface sediments in zone I (0.64–0.94 × 10^{-4}) are broadly in agreement with this range. Moreover, Hirose and Sugimura (1991) pointed out, that U/TOC ratios in sinking organic matter increase exponentially over more than one order of magnitude with increasing primary productivity. Considering the particularly high primary productivity in Peru coastal waters (Pennington et al., 2006), most of the U/TOC ratios in surface sediments (0.64–2.1 × 10^{-4}) are in agreement with a high contribution of PNU to the overall U supply. However PNU is unlikely the burial phase causing the difference between diffusive and total U accumulation in zones III and IV (Fig. 4). This is illustrated in Fig. 6, a plot of U/TOC ratios against sediment depth. The U/TOC ratios in zones I and II are either constant or increase in the top 10 cm to values of ~2.5 × 10^{-4}. This is in agreement with organic matter degradation as well as U reduction and precipitation from pore water. In contrast to that, U/TOC ratios in zone III are more heterogeneous with maximum values as high as 12 × 10^{-4} shortly below the sediment surface. These values are far too high as to be explained with PNU as the primary host phase. Consequently, some mechanism of diagenetic redistribution has to be considered. Because of strong bottom currents and the associated effects of reworking and winnowing, zone III reveals low net sedimentation rates (Table 5), which favors the formation and accumulation of phosphorite crusts

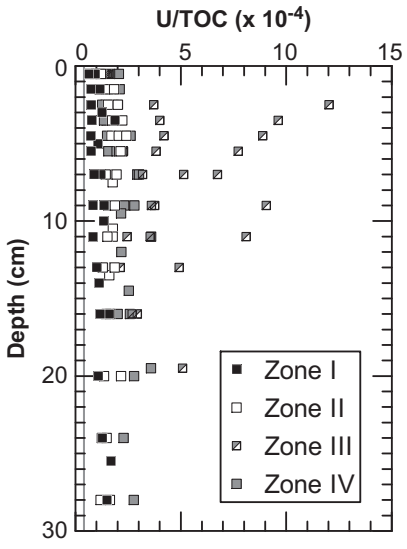

Fig. 6. Plot of U/TOC ratios versus sediment depth. The vertical gray line indicates the range of U/TOC ratios published for water column particulate matter in the NE Pacific, offshore California (Zheng et al., 2002b).

and nodules (Reimers and Suess, 1983; Glenn and Arthur, 1988). In agreement with this general observation, numerous macroscopic phosphorite concretions were recovered from the MUCs in zone III and previous studies revealed increasing P concentrations and P/C ratios across the Peruvian margin (Böning et al., 2004). Phosphorites are known to be enriched in U with respect to both the detrital background and the surrounding sediment matrix (Veeh et al., 1974; Jarvis et al., 1994) and Böning et al. (2004) reported a good correlation between U and P for a sediment core from the Peruvian slope (598 m water depth). Combining the average inorganic P concentration (i.e. corrected for the organic P content) of 1.9 wt.% reported for this core by Böning et al. (2004) with the range of U concentrations published by Arning et al. (2009) for phosphorite crusts from the Peruvian margin ($\sim$150–280 μg g^{-1} or U/P ratio of $\sim 0.9–1.7 \times 10^{-4}$) yields phosphorite-bound U concentrations of $\sim$17–32 μg U g^{-1} bulk sediment. This calculation further substantiates the assumption of Böning et al. (2004) that authigenic phosphorite is most likely an important host for U in Peru slope sediments (80–250% of the U MAR in zone III). Glenn and Arthur (1988) emphasized the role of lateral sediment transport and reorganization for the enrichment of phosphorites on the Peruvian slope. Sediment MARs increase below zone II (Table 5) leading to increasing authigenic U MARs (Fig. 4), despite a general decrease in U/Al (Fig. 5). It is therefore anticipated that much of the U buried in zones III and IV is of allochthonous origin, i.e. has originally accumulated further upslope. The ultimate origin of the phosphorite-bound U (dissolved U in pore water versus PNU) and the mode of incorporation (inorganic versus microbial mechanism) cannot be resolved based on our data. However, in consideration of the apparent imbalance between diffusive and total U supply in most areas on the Peruvian margin, at least some of the U buried is likely delivered as PNU or another, yet unidentified U phase.

4.3.2. V–Mo–U covariation in Peru upwelling sediments

The lowest authigenic MARs of V and Mo as well as the lowest V/Al and Mo/Al ratios are observed in zone IV and the deepest core in zone III (Figs. 4 and 5). This in agreement with the pore water data suggesting that redox conditions below the permanent OMZ are not reducing enough as to enable a downward benthic flux or an efficient authigenic removal of the V and Mo that is released from solid carriers. Lateral input of phosphorite-rich sediments from further upslope cannot compensate for that, since authigenic phosphorites do not sequester V or Mo to a significant extent (Jarvis et al., 1994). The small but still significant V MAR observed in zone IV might be related to lateral supply of some other authigenic V phase from further upslope or to re-adsorption of V(IV) to refractory Fe (oxyhydr)oxides. In sharp contrast to U, authigenic MARs of V and Mo are most pronounced in MUC29 in zone I where they exceed all of the benthic fluxes observed in this study. A similar mismatch between diffusive and total authigenic Mo supply has been postulated (though not proven based on pore water data) for weakly restricted basins with redox variations at short time scales (e.g. Saanich Inlet and Cariaco Basin) (Algeo and Lyons, 2006; Algeo and Tribovillard, 2009). In such settings, vertical fluctuations of the chemocline alternately promote (i) Mo scavenging by Mn and Fe (oxyhydr)oxides that precipitate in the water column during oxic periods and (ii) reductive recycling of the Mn and Fe at the sediment surface as well as sulfidation and fixation of the released Mo during anoxic periods (Berrang and Grill, 1974; Adelson et al., 2001; Algeo and Lyons, 2006). This particulate shuttle leads to an enhanced supply of particle-reactive elements as compared to those that are chiefly delivered by molecular diffusion (e.g. U) (Algeo and Tribovillard, 2009). On the Peruvian shelf, the continuous displacement of the upper boundary of the OMZ likely exerts a similar effect on Mo cycling. During periods of shelf oxygenation, surface sediments receive particulate Mo associated with terrigenous Mn and Fe (oxyhydr)oxides. This terrigenous supply is particularly pronounced during El Niño events, when otherwise arid coastal Peru receives heavy rainfall resulting in enhanced continental erosion and runoff (Wells, 1990). Moreover, additional (oxyhydr)oxides are likely supplied through reoxidation and precipitation of dissolved Mn and Fe at the retreating upper oxycline of the OMZ. After the recurrence of anoxic conditions, the (oxyhydr)oxides are reductively dissolved and recycled whereas the hereby liberated Mo is removed into authigenic phases. This scenario is in excellent agreement with the pore water Mo profile of MUC29, indicating both Mo release and authigenic removal, as well as the relatively high upward directed benthic fluxes of Mn and Fe in zone I compared to zones II and III. Moreover, a particulate shuttle, driven by ENSO-related fluctuations in bottom water oxygenation, is a viable explanation for the decoupling of U and Mo accumulation on the Peruvian shelf. However, the pore water profiles in zone I do not only indicate Mo release from metal (oxyhydr)oxides but also

Mo, V and U remobilization. Consequently, not only preferential supply but also preferential loss of specific elements has to be considered in this discussion.

Further insights into the different modes of trace metal supply versus remobilization may be obtained from cross plots of authigenic Mo versus authigenic V und U concentrations (Fig. 7). Concomitantly increasing authigenic V and Mo concentrations in zones IV and III (Fig. 7a) reflect the decreasing sediment redox potential determined by decreasing bottom water oxygen concentrations towards the core of the OMZ. MUC33 and MUC19 in zone II display a separate trend implying a relative increase in the efficiency of V accumulation. This is likely related to the abrupt TOC increase from ~5 to >10 wt.% at the transition between zones III and II (Fig. 5). Refractory organic matter is an important host phase for reduced V species (Breit and Wanty, 1991) and Algeo and Maynard (2004) reported a TOC threshold of ~7 wt.% beyond which they detected a significant increase in V accumulation in Pennsylvanian black shales. The V accumulation in zone II is likely favored by the ubiquity of refractory organic compounds providing binding sites for the reduced V in pore water. In contrast, Mo resides primarily in sulfidic phases in anoxic sediments (Huerta-Diaz and Morse, 1992; Algeo and Maynard, 2004; Tribovillard et al., 2004) and any influence of the TOC content would be rather indirect, i.e. by determining the intensity of sulfate reduction (McManus et al., 2006). The highest authigenic V and Mo concentrations are observed in BIGO-T, the shallowest core in zone II. Pore water profiles of this core indicate redox oscillations in the water column (Fig. 3) suggesting that a significant portion of the V and Mo has been shuttled by metal (oxyhydr)oxides. At the transition to zone I, however, authigenic V concentrations decrease abruptly whereas Mo concentrations in MUC29 are still higher than in most samples of zones II and III. This is unlikely due to preferential Mo supply with particulate matter, since V has a higher affinity to Mn and Fe (oxyhydr)oxides than Mo (Takematsu et al., 1985). Alternatively, reduced retention of authigenic V during oxygenation periods might be the reason for the decoupling. The major diagenetic sink of Mo is Fe sulfides (pyrite and structurally similar Mo–Fe–S phases) (Bostick et al., 2003; Vorlicek et al., 2004) whereas V does not enter sulfide minerals to a significant extent (Huerta-Diaz and Morse, 1992; Scholz and Neumann, 2007). Concentrations of TS in MUC29 are among the highest observed throughout this study. Moreover, TS is decoupled from TOC in zone I (Fig. 5), which clearly indicates enhanced preservation of sulfur with respect to organic carbon. As mentioned in Section 4.1, Suits and Arthur (2000) reported the highest pyrite concentrations and DOP values throughout the Peruvian margin (12.0–13.5°S) for sediments on the shelf. The high pyrite concentrations have been assigned to the enhanced availability of reactive Fe compounds. Furthermore, Suits and Arthur (2000) hypothesized that pyrite formation on the Peruvian shelf is particularly favored by ENSO-related redox oscillations. This is related to the enhanced formation of sulfur intermediates (S^0, $S_2O_3^{2-}$, S_n^{2-}) from H_2S under slightly oxidizing conditions, which in turn stimulates the conversion of Fe monosulfides (FeS) to pyrite via the polysulfide pathway (Schoonen and Barnes, 1991; Schoonen, 2004; Rickard and Morse, 2005). In addition, experimental work by Vorlicek et al. (2004) has revealed that polysulfides (S_n^{2-}) do also promote the conversion of $MoOS_3^{2-}$ to MoS_4^{2-}, which is the ultimate step for the long-term fixation of Mo onto authigenic pyrite. As a consequence, Mo accumulation and burial is rather favored than perturbed by transient oxygenation on the Peruvian shelf. In contrast to that, V(III) is readily oxidized to V(V) under oxic conditions leading to a destabilization of authigenic V oxides and hydroxides (Wehrli and Stumm, 1989). Another factor that potentially limits the accumulation of authigenic V on the shelf is the enhanced carbon turnover and reduced preservation of refractory organic compounds under increasingly oxic conditions (Sun et al., 1993, 2002). This assumption is corroborated by the combined observations of decreasing TOC concentrations (Fig. 5) but increasing organic matter degradation rates in the landward direction across the Peruvian shelf (Bohlen et al., in press).

The discrimating effect of redox oscillations on the long-term accumulation of different trace metals is most evident

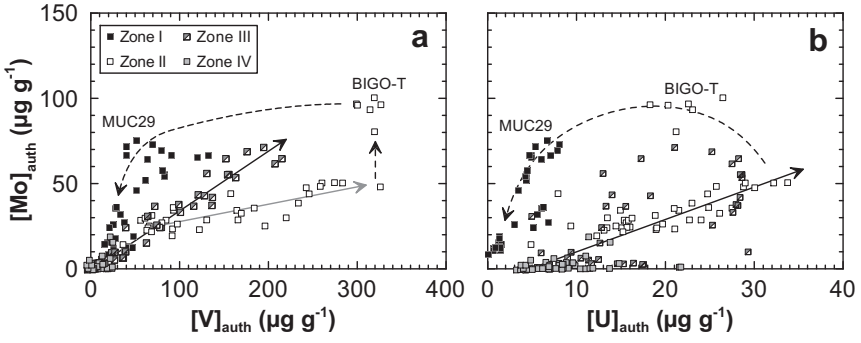

Fig. 7. Cross plot of (a) authigenic Mo concentration versus authigenic V concentration and (b) authigenic Mo concentration versus authigenic U concentration. Solid lines in (a) are linear regressions through samples in zones IV and III (black solid arrow; $R^2 = 0.95$, $n = 89$) and MUC33 and MUC19 in zone II (gray solid arrow; $R^2 = 0.72$, $n = 36$). The solid line in (b) is a linear regression though data of zones IV, III and MUC33 and MUC19 in zone II ($R^2 = 0.60$, $n = 125$). The dashed lines illustrate enhanced supply of Mo with metal (oxyhydr)oxides and remobilization of V and U in consequence of ENSO-related oxygenation events in BIGO-T and zone I. See text for further explanation.

in Fig. 7b, a cross plot of authigenic Mo versus authigenic U concentrations. Concomitantly increasing authigenic Mo and U concentrations between zone IV and MUC19 in zone II (Fig. 7b) are in agreement with the increasing diffusive benthic fluxes and reflect the decreasing benthic redox potential towards the central OMZ. At shallower depth, however, authigenic U concentrations decrease dramatically while Mo concentrations continue to increase. One reason for this decoupling is that U does not adsorb to (oxyhydr)oxides in the water column and therefore does not participate in the particulate shuttle (cp. Algeo and Tribovillard, 2009). Another reason, however, is most likely related to the strong susceptibility to re-oxidation of authigenic U. It was argued in Section 4.2.1 that pore water U profiles on the Peruvian shelf are strongly affected by remobilization. The re-oxidized and dissolved authigenic U in pore water induces an upward concentration gradient and thus impedes any additional U accumulation. Thus, the combined evidence of our pore water and sediment data strongly suggest that reduced uptake and preferential loss of U during oxygenation periods is of equal importance for the decoupling of U and Mo accumulation on the Peruvian shelf.

4.4. Implication for the use of U–Mo systematics as paleo-redox proxy

A number of studies have proposed to use Mo and U systematics to gain information about paleo-redox conditions (Algeo and Lyons, 2006; McManus et al., 2006; Algeo and Tribovillard, 2009). This approach is of great relevance for upwelling areas or other oxygen-deficient settings where recent studies have attempted to reconstruct past OMZ extension and/or ENSO variability (e.g. Nameroff et al., 2004; Gutiérrez et al., 2009; Díaz-Ochoa et al., 2011). McManus et al. (2006) derived an empirical relationship between sedimentary U/Mo ratios and oxygen concentrations in bottom water. Disregarding MUC27 at 2025 m water depth, U/Mo ratios decrease upslope across the Peruvian margin (Fig. 8) and broadly retrace the bottom water oxygen concentration at the time of sampling (Table 1). However, the corresponding correlation trend is quite different from the one presented by McManus et al. (2006)

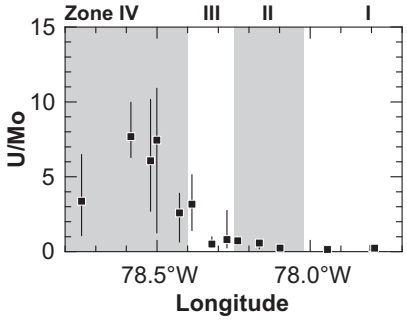

Fig. 8. Plot of U/Mo ratio versus longitude. Error bars span the range between the highest and lowest value of each core. The grayish and whitish arrays represent zone I to zone IV in Fig. 3.

(Fig. 9a) suggesting that any relationship to bottom water oxygen is of rather regional relevance. Major deviations from the trend by McManus et al. (2006) are observed in zone I where fluctuations in bottom water oxygenation enhance Mo accumulation (through particulate supply) and diminish U accumulation (through remobilization) thus pushing the U/Mo ratios to lower values. By contrast, comparably high U/Mo ratios in zones III and IV are attributed to the relative enrichment of U over Mo in authigenic phosphorites which are particularly abundant on the Peruvian slope. McManus et al. (2006) suggested that their empirical relationship is in fact due to increasing sulfate reduction rates and thus an increased availability of dissolved H_2S in pore water with decreasing oxygen concentrations in bottom water. This assumption is in agreement with our findings on U and Mo diagenesis in Peru upwelling sediments and further corroborated by the exponential relationship observed between U/Mo ratios and sediment TS (including MUC27, Fig. 9b). The non-linearity of this relationship is not surprising, given that U reduction is mediated by both Fe- and sulfate-reducing bacteria whereas authigenic Mo fixation requires the presence of H_2S. In light of these findings, U/Mo ratios in sediments or sedimentary rocks might be used to constrain whether shallow pore waters were ferruginous or (at least temporarily) sulfidic at the time of deposition. This could be also a promising approach to trace the past location of the lower boundary of the Peruvian OMZ where U/Mo ratios rapidly drop at the transition from zone IV to III (Fig. 8). However, as for the relationship between U/Mo and bottom water oxygen, variable processes of sediment redistribution on the slope may complicate the interpretation of paleo-records.

It is important to note that the use of U/Mo ratios obscures the decoupling of U with respect to Mo on the Peruvian shelf (Figs. 8 and 9), although this holds great potential for the reconstruction of past oxygen fluctuations in bottom water. Algeo and Tribovillard (2009) presented sedimentary U and Mo concentrations in cross plots of enrichment factors in order to illustrate multiple controls on U–Mo covariation in oxygen-deficient marine systems. They identified distinct arrays (dashed lines in Fig. 10) indicating (i) concomitantly increasing U and Mo accumulation with decreasing benthic redox potential in open-ocean upwelling areas and (ii) preferential accumulation of Mo over U in weakly restricted basins with a particulate shuttle in the water column. These U–Mo covariation patterns were then used to reconstruct depositional conditions in paleo-marine systems. Plotting our Mo and U data from the Peruvian margin in a cross plot of enrichment factors yields additional information on how bottom water oxygen fluctuations in open-ocean settings may affect U–Mo systematics. The trend line of shelf cores in Fig. 7b (curved arrow) appears as a straight line in Fig. 10 (linear regression through samples of zone I and BIGO-T). This line is almost identical to the trend of weakly restricted basins with a particulate shuttle in the water column of Algeo and Tribovillard (2009). We have identified a similar mechanism on the Peruvian margin. However, in contrast to restricted basins, where the chemocline fluctuates up and down, the OMZ boundaries move rather laterally across a flat shelf leading

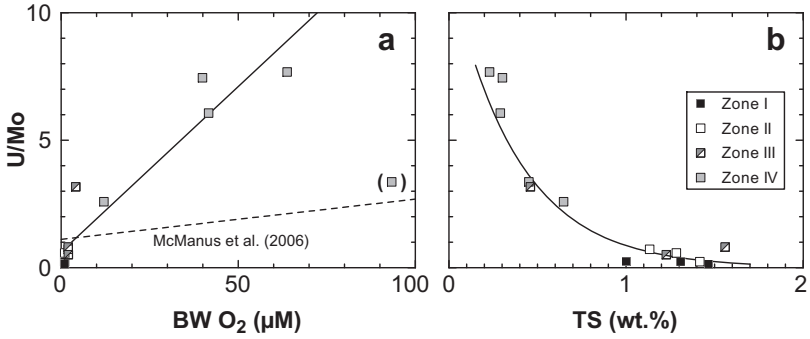

Fig. 9. Cross plots of average U/Mo ratios versus (a) bottom water (BW) oxygen concentration and (b) TS. See error bars in Figs. 5 and 8 for uncertainties. Solid black lines represent linear ($R^2 = 0.90$, $n = 13$) or exponential fits ($R^2 = 0.83$, $n = 14$) (MUC27 is shown in parentheses in (a) and has not been considered in the fit). The black dashed line in (a) represents the empirical relationship between U/Mo ratio and BW oxygen concentration in hypoxic marine settings by McManus et al. (2006).

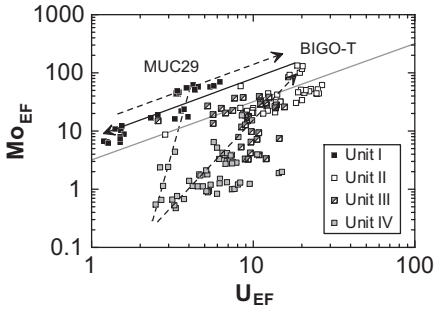

Fig. 10. Cross plot of Mo enrichment factors versus U enrichment factors. The metal enrichment factor is defined as $Me_{EF} = [Me]_{tot}/[Al]_{tot}/[Me]_{detr}/[Al]_{detr}$ where the index 'detr' refers to the detrital background (andesite in the Andean Arc, see Table 2). Note the logarithmic scale of both axes. The solid gray line depicts the relative proportion of Mo and U in seawater (weight ratio of $[Mo]_{sw}/[U]_{sw} = 3.2$). The dashed lines are adapted from Algeo and Tribovillard (2009) and illustrate a decreasing sediment redox potential in open marine systems (straight arrow) and enhanced Mo supply with metal (oxyhydr)oxides (i.e. a particulate shuttle) in weakly restricted basins (branched arrow). The solid black arrow is a linear regression through samples in zone I and BIGO-T in zone II ($R^2 = 0.82$, $n = 38$). See text for further explanation.

to a transition between areas where mostly oxic and others where mostly anoxic conditions in bottom water prevail. Although enhanced Mo supply with coated particulates is an important aspect of this environment, preferential loss of U during oxic periods is almost certainly of equal importance for the characteristic U–Mo pattern observed. Keeping that in mind, cross plots of Mo versus U like those in Figs. 7b and 10 could be of great use for the reconstruction of past OMZ variability and redox oscillations in ancient open-ocean environments in general.

5. SUMMARY AND CONCLUSIONS

We have investigated the spatial and temporal variability of trace metal diagenesis (U, V and Mo) across the Peru upwelling area. Our findings are summarized in a conceptual model consisting of two end member situations that correspond to negative (La Niña) and positive (El Niño) ENSO conditions (Fig. 11).

A: Within the permanent OMZ, U, V and Mo diffuse across the sediment/bottom water interface and precipitate in the zones of Fe and sulfate reduction. Since Mn reduction is largely completed in the water column, sediments receive little Mn-bound, particulate V and Mo. This favors the establishment of a downward directed benthic V and Mo flux. Because of the permanently anoxic but non-sulfidic conditions in the bottom water, surface sediments within the OMZ are subject to a continuous diffusive loss of Fe. Some of the dissolved Mn and Fe in the water column are re-precipitated at the oxyclines and deposited at the lower and upper boundary of the OMZ.

B: Sediments below the OMZ receive particulate V and Mo with metal (oxyhydr)oxides that have precipitated at the lower oxycline. This particulate V and Mo is released into the pore water upon Mn and Fe reduction. Since pore waters below the OMZ are generally not sufficiently sulfidic for an efficient authigenic removal, most of the liberated V and Mo is lost through upward diffusion across the benthic boundary. Intense U accumulation below the OMZ is attributed to both in situ reduction of U in the Fe reduction zone and lateral input of U-rich phosphorites from further upslope. The long term accumulation of V, Mo and U below the OMZ is diminished by the activity of bioturbating and bioirrigating organisms.

C: Sediments on the Peruvian shelf are strongly affected by ENSO-related oxygen fluctuations in bottom water. During positive ENSO periods, when bottom waters on the shelf are oxic, terrigenous Mn and Fe (oxyhydr)oxides as well as metal (oxyhydr)oxides that have precipitated at the retreating oxycline shuttle V and Mo to the sediment surface. After the recurrence of anoxic conditions, the Mn and Fe (oxyhydr)oxides are reductively recycled thus leading to high benthic Mn and Fe fluxes as compared to the

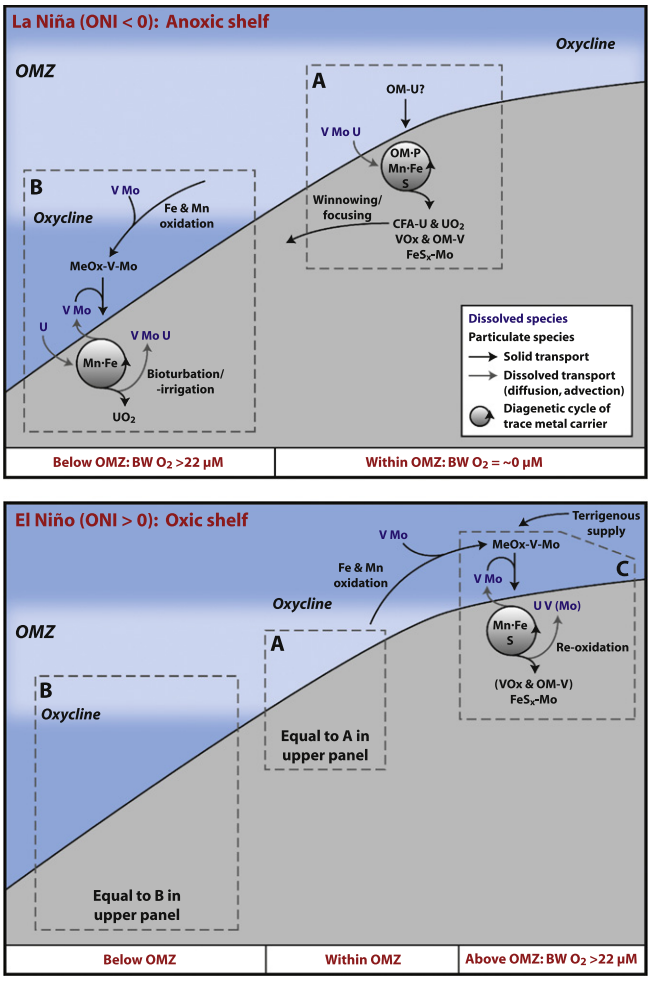

Fig. 11. Conceptual model for trace metal cycling across the Peruvian continental margin during two end member situations corresponding to negative (La Niña) and positive (El Niño) ENSO conditions. The abbreviations are as follows: MeOx = metal (oxyhydr)oxides, OM = organic matter, CFA = phosphorites (calcium fluoride apatite), VOx = V(III) oxides and hydroxides, FeS_x = Fe sulfides. See text for a detailed explanation of the biogeochemical processes in A, B and C.

permanent OMZ. Upon dissolution of the particulate carriers, the adsorbed V and Mo are released into the pore water and authigenically removed in the sulfate reduction zone. This alternation between supply of particle-reactive trace metals during oxic periods and authigenic fixation during anoxic periods leads to a preferential accumulation of V and Mo over U on the Peruvian shelf. The decoupling between V, Mo and U accumulation is further accentuated by the varying susceptibility to re-oxidation of the different authigenic metal phases. While authigenic V and U are readily re-oxidized and recycled during oxygenation periods, Mo accumulation with authigenic pyrite is favored by the occasional occurrence of slightly oxidizing conditions.

ENSO-related redox fluctuations in bottom water are likely to affect metal cycling along the entire SE Pacific ocean margin and similar phenomena might have occurred in ancient oceans through earth history. This study reveals that relative enrichments and/or depletions of redox-sensitive trace metals (most notably Mo and U) are sensitive to short-term fluctuations in bottom water oxygenation. The next step will be to apply this concept downcore in order to reconstruct past OMZ extension and variability as well as to identify large-scale redox fluctuations in the geological record.

ACKNOWLEDGMENTS

We are indebted to the IFM-GEOMAR technicians A. Bleyer, M. Dibbern, B. Domeyer, R. Ebbinghaus, A. Petersen and R. Surberg for their enthusiastic help and cooperation during the M77 cruises and the post-cruise work in Kiel. Furthermore, we would like to thank the officers and crew of RV Meteor for their commitment during the sampling campaign. Constructive and insightful comments from Thomas J. Algeo, Nicolas Tribovillard and one anonymous reviewer as well as from the associate editor, George R. Helz, are greatly appreciated. This work is a contribution of the Sonderforschungsbereich 754 "Climate-Biogeochemistry Interactions in the Tropical Ocean" (www.sfb754.de/en/) which is supported by the Deutsche Forschungsgemeinschaft.

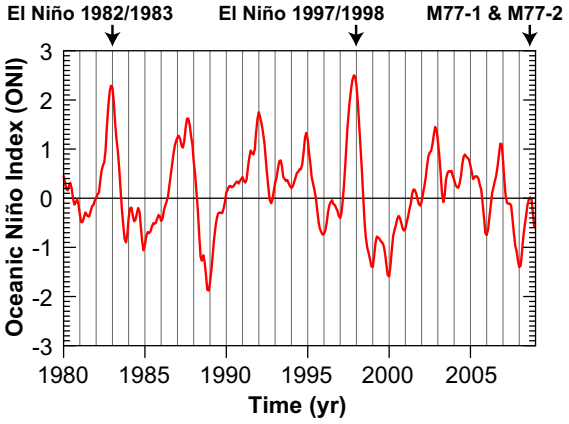

Fig. A1. Time series of the Oceanic Niño Index (ONI) between 1980 and 2008 (data from the U.S. National Oceanic and Atmospheric Administration, NOAA). The ONI is defined as the three monthly running mean of the sea surface temperature anomaly in the Niño 3.4 region (5°N–5°S, 120°–170°W). The strong El Niño events of 1982/1983 and 1997/1998 as well as the period of the research cruises M77-1 and M77-2 are indicated by vertical arrows. In general, positive ONI periods are associated with warmer temperatures and frequent shelf oxygenation whereas negative ONI periods are associated with lower temperatures and shelf anoxia.

APPENDIX A

APPENDIX B. SUPPLEMENTARY DATA

Supplementary data associated with this article can be found, in the online version, at doi:10.1016/j.gca.2011.08.007.

REFERENCES

Adelson J. M., Helz G. R. and Miller C. V. (2001) Reconstructing the rise of recent coastal anoxia; molybdenum in Chesapeake Bay sediments. *Geochim. Cosmochim. Acta* **65**, 237–252.

Algeo T. J. and Maynard J. B. (2004) Trace-element behavior and redox facies in core shales of Upper Pennsylvanian Kansas-type cyclothems. *Chem. Geol.* **206**, 289–318.

Algeo T. J. and Lyons T. W. (2006) Mo-total organic carbon covariation in modern anoxic marine environments: implications for analysis of paleoredox and paleohydrographic conditions. *Paleoceanography* **21**, PA1016. doi:10.1029/2004PA001112.

Algeo T. J. and Tribovillard N. (2009) Environmental analysis of paleoceanographic systems based on molybdenum–uranium covariation. *Chem. Geol.* **268**, 211–225.

Anderson R. F. (1982) Concentration, vertical flux, and remineralization of particulate uranium in seawater. *Geochim. Cosmochim. Acta* **46**, 1293–1299.

Anderson R. F., Lehuray A. P., Fleisher M. Q. and Murray J. W. (1989a) Uranium deposition in Saanich Inlet sediments, Vancouver Island. *Geochim. Cosmochim. Acta* **53**, 2205–2213.

Anderson R. F., Fleisher M. Q. and LeHuray A. P. (1989b) Concentration, oxidation state, and particulate flux of uranium in the Black Sea. *Geochim. Cosmochim. Acta* **53**, 2215–2224.

Arning E. T., Lückge A., Breuer C., Gussone N., Birgel D. and Peckmann J. (2009) Genesis of phosphorite crusts off Peru. *Mar. Geol.* **262**, 68–81.

Audry S., Blanc G., Schäfer J., Chaillou G. and Robert S. (2006) Early diagenesis of trace metals (Cd, Cu, Co, Ni, U, Mo, and V) in the freshwater reaches of a macrotidal estuary. *Geochim. Cosmochim. Acta* **70**, 2264–2282.

Barling J. and Anbar A. D. (2004) Molybdenum isotope fractionation during adsorption by manganese oxides. *Earth Planet. Sci. Lett.* **217**, 315–329.

Barnes C. E. and Cochran J. K. (1990) Uranium removal in oceanic sediments and the oceanic U balance. *Earth Planet. Sci. Lett.* **97**, 94–101.

Barnes C. E. and Cochran J. K. (1991) Geochemistry of uranium in Black Sea sediments. *Deep-Sea Res.* **38**, 1237–1254.

Berrang P. G. and Grill E. V. (1974) The effect of manganese oxide scavenging on molybdenum in Saanich Inlet, British Columbia. *Mar. Chem.* **2**, 125–148.

Bohlen L., Dale A. W., Sommer S., Mosch T., Hensen C., Noffke A., Scholz F. and Wallmann K. (2011) Benthic nitrogen cycling traversing the Peruvian oxygen minimum zone. *Geochim. Cosmochim. Acta.* **75**, 7257–7276.

Böning P., Brumsack H. J., Böttcher M. E., Schnetger B., Kriete C., Kallmeyer J. and Borchers S. L. (2004) Geochemistry of Peruvian near-surface sediments. *Geochim. Cosmochim. Acta* **68**, 4429–4451.

Böning P., Brumsack H. J., Schnetger B. and Grunwald M. (2009) Trace element signatures of Chilean upwelling sediments at 36 S. *Mar. Geol.* **259**, 112–121.

Bostick B. C., Fendorf S. and Helz G. R. (2003) Differential adsorption of molybdate and tetrathiomolybdate on pyrite (FeS_2). *Env. Sci. Technol.* **37**, 285–291.

Boudreau B. P. (1996) The diffusive tortuosity of fine-grained unlithified sediments. *Geochim. Cosmochim. Acta* **60**, 3139–3142.

Breit G. N. and Wanty R. B. (1991) Vanadium accumulation in carbonaceous rocks: a review of geochemical controls during deposition and diagenesis. *Chem. Geol.* **91**, 83–97.

Brink K. H. (1982) A Comparison of long coastal trapped wave theory with observations off Peru. *J. Phys. Oceanogr.* **12**, 897–913.

Bruland A. et al. (1983) Trace elements in seawater. In *Chemical oceanography*, vol. 8 (eds. J. P. Riley and R. Chester), pp. 157–220. Chemical oceanography. Academic Press, London.

Bruland K. W., Rue E. L., Smith G. J. and DiTullio G. R. (2005) Iron, macronutrients and diatom blooms in the Peru upwelling regime: brown and blue waters of Peru. *Mar. Chem.* **93**, 81–103.

Brumsack H. J. and Gieskes J. M. (1983) Interstitial water trace-metal chemistry of laminated sediments from the Gulf of California, Mexico. *Mar. Chem.* **14**, 89–106.

Brumsack H. J. (2006) The trace metal content of recent organic carbon-rich sediments: implications for Cretaceous black shale formation. *Paleogeogr. Palaeocl.* **232**, 344–361.

Burdige D. J. (1993) The biogeochemistry of manganese and iron reduction in marine-sediments. *Earth-Sci. Rev.* **35**, 249–284.

Calvert S. E. and Pedersen T. F. (1993) Geochemistry of recent oxic and anoxic marine sediments: implications for the geological record. *Mar. Geol.* **113**, 67–88.

Chaillou G., Anschutz P., Lavaux G., Schäfer J. and Blanc G. (2002) The distribution of Mo, U, and Cd in relation to major redox species in muddy sediments of the Bay of Biscay. *Mar. Chem.* **80**, 41–59.

Chan K. M. and Riley J. P. (1966a) The determination of molybdenum in natural waters, silicates and biological materials. *Anal. Chim. Acta* **36**, 220–229.

Chan K. M. and Riley J. P. (1966b) The determination of vanadium in sea and natural waters, biological materials and silicate sediments and rocks. *Anal. Chim. Acta* **34**, 337–345.

Díaz-Ochoa J. A., Pantoja S., De Lange G. J., Lange C. B., Sánchez G. E., Acuña V. R., Muñoz P. and Vargas G. (2011) Oxygenation variability in Mejillones Bay, off northern Chile, during the last two centuries. *Biogeosciences* **8**, 137–146.

Diaz R. J. (2001) Overview of Hypoxia around the World. *J. Environ. Qual.* **30**, 275–281.

Diaz R. J. and Rosenberg R. (2008) Spreading dead zones and consequences for marine ecosystems. *Science* **321**, 926–929.

Emerson S. R. and Huested S. S. (1991) Ocean anoxia and the concentrations of molybdenum and vanadium in seawater. *Mar. Chem.* **34**, 177–196.

Erickson B. E. and Helz G. R. (2000) Molybdenum(VI) speciation in sulfidic waters: stability and lability of thiomolybdates. *Geochim. Cosmochim. Acta* **64**, 1149–1158.

Froelich P. N., Klinkhammer G. P., Bender M. L., Luedtke N. A., Heath G. R., Cullen D., Dauphin P., Hammond D., Hartman B. and Maynard V. (1979) Early oxidation of organic matter in pelagic sediments of the eastern equatorial Atlantic: suboxic diagenesis. *Geochim. Cosmochim. Acta* **43**, 1075–1090.

Fuenzalida R., Schneider W., Garcés-Vargas J., Bravo L. and Lange C. (2009) Vertical and horizontal extension of the oxygen minimum zone in the eastern South Pacific Ocean. *Deep-Sea Res.* **56**, 992–1003.

Glenn C. R. and Arthur M. A. (1988) Petrology and major element geochemistry of Peru margin phosphorites and associated diagenetic minerals: authigenesis in modern organic-rich sediments. *Mar. Geol.* **80**, 231–267.

Goldberg T., Archer C., Vance D. and Poulton S. W. (2009) Mo isotope fractionation during adsorption to Fe (oxyhydr)oxides. *Geochim. Cosmochim. Acta* **73**, 6502–6516.

Govindaraju K. (1994) Compilation of working values and sample description for 383 geostandards. *Geostandard Newslett.* **18**, 1–158.

Grasshoff K., Erhardt M. and Kremling K. (2002) *Methods of Seawater Analysis*. Wiley-VCH, Weinheim.

Gutiérrez D., Gallardo V. A., Mayor S., Neira C., Vasquez C., Sellanes J., Rivas M., Soto A., Carrasco F. and Baltazar M. (2000) Effects of dissolved oxygen and fresh organic matter on the bioturbation potential of macrofauna in sublittoral sediments off Central Chile during the 1997/1998 El Niño. *Mar. Ecol.-Prog. Ser.* **202**, 81–99.

Gutiérrez D., Enríquez E., Purca S., Quipúzcoa L., Marquina R., Flores G. and Graco M. (2008) Oxygenation episodes on the continental shelf of central Peru: remote forcing and benthic ecosystem response. *Prog. Oceanogr.* **79**, 177–189.

Gutiérrez D., Sifeddine A., Field D. B., Ortlieb L., Vargas G., Chavez F. P., Velazco F., Ferreira V., Tapia P., Salvatteci R., Boucher H., Morales M. C., Valdes J., Reyss J. L., Campusano A., Boussafir M., Mandeng-Yogo M., Garcia M. and Baumgartner T. (2009) Rapid reorganization in ocean biogeochemistry off Peru towards the end of the Little Ice Age. *Biogeosciences* **6**, 835–848.

Helz G. R., Miller C. V., Charnock J. M., Mosselmans J. F. W., Pattrick R. A. D., Garner C. D. and Vaughan D. J. (1996) Mechanism of molybdenum removal from the sea and its concentration in black shales: EXAFS evidence. *Geochim. Cosmochim. Acta* **60**, 3631–3642.

Hirose K. and Sugimura Y. (1991) Chemical speciation of particulate uranium in seawater. *J. Radioanal. Nucl. Chem.* **149**, 83–96.

Hormazabal S., Shaffer G., Letelier J. and Ulloa O. (2001) Local and remote forcing of sea surface temperature in the coastal upwelling system off Chile. *J. Geophys. Res.* **106**, 16657–16671.

Huerta-Diaz M. A. and Morse J. W. (1992) Pyritization of trace metals in anoxic marine sediments. *Geochim. Cosmochim. Acta* **56**, 2681–2702.

Jarvis I., Burnett W. C., Nathan Y., Almbaydin F. S. M., Attia A. K. M., Castro L. N., Flicoteaux R., Hilmy M. E., Husain V., Qutawnah A. A., Serjani A. and Zanin Y. N. (1994) Phosphorite geochemistry – state of the art and environmental concerns. *Eclogae Geol. Helv.* **87**, 643–700.

Klinkhammer G. P. and Palmer M. R. (1991) Uranium in the oceans – where it goes and why. *Geochim. Cosmochim. Acta* **55**, 1799–1806.

Levin L., Gutiérrez D., Rathburn A., Neira C., Sellanes J., Muñoz P., Gallardo V. and Salamanca M. (2002) Benthic processes on the Peru margin: a transect across the oxygen minimum zone during the 1997–98 El Niño. *Prog. Oceanogr.* **53**, 1–27.

Li Y.-H. and Gregory S. (1974) Diffusion of ions in sea water and in deep-sea sediments. *Geochim. Cosmochim. Acta* **38**, 703–714.

Liger E., Charlet L. and Van Cappellen P. (1999) Surface catalysis of uranium(VI) reduction by iron(II). *Geochim. Cosmochim. Acta* **63**, 2939–2955.

Lovley D. R. and Phillips E. J. (1992) Reduction of uranium by *Desulfovibrio desulfuricans*. *Appl. Environ. Microbiol.* **58**, 850–856.

Lovley D. R., Phillips E. J. P., Gorby Y. A. and Landa E. R. (1991) Microbial reduction of uranium. *Nature* **350**, 413–416.

Lovley D. R., Roden E. E., Phillips E. J. P. and Woodward J. C. (1993) Enzymatic iron and uranium reduction by sulfate-reducing bacteria. *Mar. Geol.* **113**, 41–53.

McLennan S. M. (2001) Relationships between the trace element composition of sedimentary rocks and upper continental crust. *Geochem. Geophys. Geosyst.* 2, paper number 2000GC000109.

McManus J., Berelson W. M., Klinkhammer G. P., Hammond D. E. and Holm C. (2005) Authigenic uranium: relationship to oxygen penetration depth and organic carbon rain. *Geochim. Cosmochim. Acta* **69**, 95–108.

McManus J., Berelson W. M., Severmann S., Poulson R. L., Hammond D. E., Klinkhammer G. P. and Holm C. (2006) Molybdenum and uranium geochemistry in continental margin sediments: paleoproxy potential. *Geochim. Cosmochim. Acta* **70**, 4643–4662.

Meysman F. J. R., Boudreau B. P. and Middelburg J. J. (2005) Modeling reactive transport in sediments subject to bioturbation and compaction. *Geochim. Cosmochim. Acta* **69**, 3601–3617.

Middelburg J. J. and Levin L. A. (2009) Coastal hypoxia and sediment biogeochemistry. *Biogeosciences* **6**, 1273–1293.

Morford J. L., Emerson S. R., Breckel E. J. and Kim S. H. (2005) Diagenesis of oxyanions (V, U, Re, and Mo) in pore waters and sediments from a continental margin. *Geochim. Cosmochim. Acta* **69**, 5021–5032.

Morford J. L., Martin W. R. and Carney C. M. (2009a) Uranium diagenesis in sediments underlying bottom waters with high oxygen content. *Geochim. Cosmochim. Acta* **73**, 2920–2937.

Morford J. L., Martin W. R., François R. and Carney C. M. (2009b) A model for uranium, rhenium, and molybdenum diagenesis in marine sediments based on results from coastal locations. *Geochim. Cosmochim. Acta* **73**, 2938–2960.

Nameroff T. J., Balistrieri L. S. and Murray J. W. (2002) Suboxic trace metal geochemistry in the Eastern Tropical North Pacific. *Geochim. Cosmochim. Acta* **66**, 1139–1158.

Nameroff T. J., Calvert S. E. and Murray J. W. (2004) Glacial-interglacial variability in the Eastern Tropical North Pacific oxygen minimum zone recorded by redox-sensitive trace metals. *Paleoceanography* **19**, PA1010. doi:10.1029/2003PA000912.

Noffke A., Hensen C., Sommer S., Croot P., Scholz F., and Wallmann K. (2011) The benthic iron and phosphorus source across the Peruvian oxygen minimum zone. *ASLO 2011 – Aquatic Sciences Meeting*, Book of Abstracts, p. 183 (abstr.).

Pakhomova S. V., Hall P. O. J., Kononets M. Y., Rozanov A. G., Tengberg A. and Vershinin A. V. (2007) Fluxes of iron and manganese across the sediment–water interface under various redox conditions. *Mar. Chem.* **107**, 319–331.

Pennington J. T., Mahoney K. L., Kuwahara V. S., Kolber D. D., Calienes R. and Chavez F. P. (2006) Primary production in the eastern tropical Pacific: a review. *Prog. Oceanogr.* **69**, 285–317.

Pizarro O., Clarke A. J. and Van Gorder S. (2001) El Niño sea level and currents along the South American coast: comparison of observations with theory. *J. Phys. Oceanogr.* **31**, 1891–1903.

Reimers C. E. and Suess E. (1983) Spatial and temporal patterns of organic matter accumulation on the Peru continental margin. In *Coastal Upwelling: Part B. Sedimentary Record of Ancient Coastal Upwelling* (eds. E. Suess and J. Thiede). Plenum Press, New York, NY., pp. 311–346.

Rickard D. and Morse J. W. (2005) Acid volatile sulfide (AVS). *Mar. Chem.* **97**, 141–197.

Sarbas B. and Nohl U. (2009) The GEOROC database – a decade of "online geochemistry". *Geochim. Cosmochim. Acta* **73**, A1158.

Scheidegger K. F. and Krissek L. A. (1983) Zooplankton and nekton: natural barriers to the seaward transport of suspended terrigenous particles off Peru. In *Coastal Upwelling: Part A. Responses of the Sedimentary Regime to Present Coastal Upwelling* (eds. E. Suess and J. Thiede). Plenum Press, New York, NY., pp. 303–336.

Scholz F. and Neumann T. (2007) Trace element diagenesis in pyrite-rich sediments of the Achterwasser lagoon, SW Baltic Sea. *Mar. Chem.* **107**, 516–532.

Schoonen M. A. A. and Barnes H. L. (1991) Reactions forming pyrite and marcasite from solution: II. Via FeS precursors below 100 °C. *Geochim. Cosmochim. Acta* **55**, 1505–1514.

Schoonen M. A. A. (2004) Mechanisms of sedimentary pyrite formation. In *Sulfur biogeochemistry – past, present)* (eds. J. P. Amend, K. J. Edwards and T. W. Lyons). Geological Society of America Special Paper 379, Boulder, CO, pp. 117–134.

Severmann S., McManus J., Berelson W. M. and Hammond D. E. (2010) The continental shelf benthic iron flux and its isotope composition. *Geochim. Cosmochim. Acta* **74**, 3984–4004.

Shaw T. J., Gieskes J. M. and Jahnke R. A. (1990) Early diagenesis in differing depositional environments: the response of transition metals in pore water. *Geochim. Cosmochim. Acta* **54**, 1233–1246.

Shaw T. J., Sholkovitz E. R. and Klinkhammer G. (1994) Redox dynamics in the Chesapeake Bay: the effect on sediment/water uranium exchange. *Geochim. Cosmochim. Acta* **58**, 2985–2995.

Shimmield G. B. and Price N. B. (1986) The behavior of molybdenum and manganese during early sediment diagenesis – offshore Baja California, Mexico. *Mar. Chem.* **19**, 261–280.

Sommer S., Pfannkuche O., Linke P., Luff R., Greinert J., Drews M., Gubsch S., Pieper M., Poser M. and Viergutz T. (2006) Efficiency of the benthic filter: biological control of the emission of dissolved methane from sediments containing shallow gas hydrates at Hydrate Ridge. *Global Biogeochem. Cy.* **20**, GB2019. doi:10.1029/2004GB002389.

Soto-Mardones L., Parés-Sierra A. and Durazo R. (2004) Ekman modulation of the sea-surface temperature on the Eastern South Pacific. *Deep-Sea Res.* **51**, 551–561.

Stookey L. L. (1970) Ferrozine – a new spectrophotometric reagent for iron. *Anal. Chem.* **42**, 779–781.

Stramma L., Johnson G. C., Sprintall J. and Mohrholz V. (2008) Expanding oxygen-minimum zones in the tropical oceans. *Science* **320**, 655–658.

Strub P. T., Mesías J. M., Montecino V., Rutllant J., and Salinas S. (1998) Coastal ocean circulation off Western South America. In *The Sea* (eds. A. R. Robinson and K. H. Brink). John Wiley & Sons, New York, NY. pp. 273–313.

Suits N. S. and Arthur M. A. (2000) Sulfur diagenesis and partitioning in Holocene Peru shelf and upper slope sediments. *Chem. Geol.* **163**, 219–234.

Sun M.-Y., Lee C. and Aller R. C. (1993) Laboratory studies of oxic and anoxic degradation of chlorophyll-*a* in Long Island Sound sediments. *Geochim. Cosmochim. Acta* **57**, 147–157.

Sun M.-Y., Aller R. C., Lee C. and Wakeham S. G. (2002) Effects of oxygen and redox oscillation on degradation of cell-associated lipids in surficial marine sediments. *Geochim. Cosmochim. Acta* **66**, 2003–2012.

Suzuki Y., Kelly S. D., Kemner K. M. and Banfield J. F. (2005) Direct microbial reduction and subsequent preservation of uranium in natural near-surface sediment. *Appl. Environ. Microb.* **71**, 1790–1797.

Takematsu N., Sato Y. and Okabe S. (1985) The partition of vanadium and molybdenum between manganese oxides and seawater. *Geochim. Cosmochim. Acta* **49**, 2395–2399.

Taylor S. R. and McLennan S. M. (1985) *The continental crust: its composition and evolution*. Blackwell, Oxford.

Tribovillard N., Riboulleau A., Lyons T. and Baudin F. (2004) Enhanced trapping of molybdenum by sulfurized organic matter of marine origin in Mesozoic limestones and shales. *Chem. Geol.* **213**, 385–401.

Tribovillard N., Algeo T. J., Lyons T. and Riboulleau A. (2006) Trace metals as paleoredox and paleoproductivity proxies: an update. *Chem. Geol.* **232**, 12–32.

Van der Weijden C. H., Reichart G. J. and Visser H. J. (1999) Enhanced preservation of organic matter in sediments deposited within the oxygen minimum zone in the northeastern Arabian Sea. *Deep-Sea Res.* **46**, 807–830.

Veeh H. H., Calvert S. E. and Price N. B. (1974) Accumulation of uranium in sediments and phosphorites on the South West African shelf. *Mar. Chem.* **2**, 189–202.

Vorlicek T. P., Kahn M. D., Kasuya Y. and Helz G. R. (2004) Capture of molybdenum in pyrite-forming sediments: role of ligand-induced reduction by polysulfides. *Geochim. Cosmochim. Acta* **68**, 547–556.

Wanty R. B. and Goldhaber M. B. (1992) Thermodynamics and kinetics of reactions involving vanadium in natural systems: accumulation of vanadium in sedimentary rocks. *Geochim. Cosmochim. Acta* **56**, 1471–1483.

Wehrli B. and Stumm W. (1989) Vanadyl in natural waters: adsorption and hydrolysis promote oxygenation. *Geochim. Cosmochim. Acta* **53**, 69–77.

Wells L. E. (1990) Holocene history of the El Nino phenomenon as recorded in flood sediments of northern Peru. *Geology* **18**, 1134–1137.

Zheng Y., Anderson R. F., van Geen A. and Kuwabara J. (2000) Authigenic molybdenum formation in marine sediments: a link to pore water sulfide in the Santa Barbara Basin. *Geochim. Cosmochim. Acta* **64**, 4165–4178.

Zheng Y., Anderson R. F., Van Geen A. and Fleisher M. Q. (2002a) Remobilization of authigenic uranium in marine sediments by bioturbation. *Geochim. Cosmochim. Acta* **66**, 1759–1772.

Zheng Y., Anderson R. F., Van Geen A. and Fleisher M. Q. (2002b) Preservation of particulate non-lithogenic uranium in marine sediments. *Geochim. Cosmochim. Acta* **66**, 3085–3092.

Associate editor: George R. Helz